
A Unified View of Stochastic Hamiltonian Sampling

Giulio Franzese
EURECOM Data Science Department
Biot (France)

Dimitrios Milios
EURECOM Data Science Department
Biot (France)

Maurizio Filippone
EURECOM Data Science Department
Biot (France)

Pietro Michiardi
EURECOM Data Science Department
Biot (France)

Abstract

In this work, we revisit the theoretical properties of Hamiltonian stochastic differential equations (SDEs) for Bayesian posterior sampling, and we study the two types of errors that arise from numerical SDE simulation: the discretization error and the error due to noisy gradient estimates in the context of data subsampling. We consider overlooked results describing the ergodic convergence rates of numerical integration schemes, and we produce a novel analysis for the effect of mini-batches through the lens of differential operator splitting. In our analysis, the stochastic component of the proposed Hamiltonian SDE is decoupled from the gradient noise, for which we make no normality assumptions. This allows us to derive interesting connections among different sampling schemes, including the original Hamiltonian Monte Carlo (HMC) algorithm, and explain their performance. We show that for a careful selection of numerical integrators, both errors vanish at a rate $\mathcal{O}(\eta^2)$, where η is the integrator step size. Our theoretical results are supported by an empirical study on a variety of regression and classification tasks for Bayesian neural networks.

1 Introduction

Hamiltonian Monte Carlo (HMC) is a popular Markov chain Monte Carlo (MCMC) approach to obtain samples from intractable distributions, which appear in the Bayesian treatment of several complex nonlinear statistical models [39; 40; 23]. The sampling process is defined as a randomized simulation of a Hamiltonian system, which allows for a more efficient exploration of the parameter space compared to approaches based purely on random walks, such as the Metropolis-Hastings algorithm. HMC presents significant computational challenges for large datasets, as it requires access to the full gradient of the associated Hamiltonian system. Stochastic-Gradient HMC (SGHMC) [10] was proposed as a scalable alternative to HMC, by admitting noisy estimates of the gradient using mini-batching. In SGHMC, the Hamiltonian dynamics is modified so as to include a friction term that counteracts the effects of the gradient noise. This approach has proven effective in dealing with the difficulties in sampling from the posterior distribution over model parameters of Bayesian Neural/Convolutional Networks (BNNs) [51; 48].

Stochastic gradient (SG) methods have been extensively studied as a means for MCMC-based algorithms to scale to large data. Variants of SG-MCMC algorithms have been studied through the lenses of first [50; 3; 41] or second-order [10; 32] Langevin dynamics; these are mathematically convenient continuous-time processes which correspond to discrete-time gradient methods with and without momentum, respectively. The stochastic processes described by stochastic differential equations (SDE) have been intensively studied [27; 14], with some of the authors putting a particular emphasis on the stationary property of these processes [1; 35]. As in [1; 2], we are interested in the asymptotic

(in time) performance of such sampling schemes. The reader is referred to [49; 20; 19; 18; 52] for additional insights into the non asymptotic behavior of these methods.

In this work, we seek to re-evaluate the connections between SG and stochastic Hamiltonian dynamics with the aim of improving our current understanding of the goodness of sampling from intractable distributions when considering mini-batching. More specifically, we consider a system with potential $U(\boldsymbol{\theta})$ which is the negative of the logarithm of the distribution we aim to sample from. We then introduce a position term $\boldsymbol{\theta} \in \mathbb{R}^d$ (i.e., parameters) and a momentum term $\mathbf{r} \in \mathbb{R}^d$ obeying the following SDE:

$$\begin{aligned} d\mathbf{r}(t) &= -\nabla_{\boldsymbol{\theta}} U(\boldsymbol{\theta}(t))dt - C\mathbf{M}^{-1}\mathbf{r}(t)dt + \sqrt{2C}d\mathbf{w}(t) \\ d\boldsymbol{\theta}(t) &= \mathbf{M}^{-1}\mathbf{r}(t)dt. \end{aligned} \tag{1}$$

which is an extension of an Hamiltonian system with a friction term and an appropriately scaled Brownian motion $\mathbf{w}(t)$, where $C > 0$ ¹ and \mathbf{M} is a symmetric, positive definite matrix (a.k.a. mass matrix). A common assumption, shared among many works in the literature, is that the Brownian motion term can adequately model the noise associated with stochastic estimates of $\nabla_{\boldsymbol{\theta}} U(\boldsymbol{\theta}(t))$.

In this work we challenge this assumption and we advocate that SG should be completely decoupled from the SDE dynamics. In this sense, our framework is similar to [9]; however we propose an interpretation of the effect of mini-batching through the lenses of differential operator splitting, by leveraging the huge literature concerning the simulation of high dimensional Hamiltonian systems [13; 45; 22; 12; 31]. Earlier attempts [4; 42] to use operator splitting as a tool to describe mini-batching focus on HMC, whereas SGHMC and related schemes have never been studied, to the best of our knowledge, under this formalism.

Our main contribution can be summarized as the derivation of new convergence results considering the two types of error induced by the simulation of the proposed SDE scheme: the discretization and the SG errors. The discretization of SDEs has been extensively studied in the literature [27; 14; 1; 35]. In Section 2, we leverage these results to present quantitatively precise claims about sampling schemes in the context of Bayesian inference for modern machine learning problems. In Section 3, our treatment of mini-batches in terms of differential operator splitting does not rely on Gaussian assumptions regarding the form of the noise (see also Appendix A for an extended discussion). We show that for a careful selection of numerical integrator, both errors vanish at a rate $O(\eta^2)$ where η is the step size of the integrator. Thus we interpret the undeniable empirical success of methods such as SGHMC [44; 51] under a new light.

Our second contribution (Section 4) is a reinterpretation of the HMC algorithm as an integrator for Hamiltonian SDEs [1]. The exact comparison of the convergence rates of HMC with partial momentum refreshment [40; 25] with respect to the proposed SDE formalism shows that although both approaches are of order $O(\eta^2)$, the constants are significantly larger for the former approach, which translates to poorer performance. Furthermore, we provide interesting insights into the behavior of the classical HMC scheme which explain our experimental findings.

In Section 5, we conduct an extensive experimental campaign that corroborates our theory on the convergence rate of various Hamiltonian-based SDE schemes, by exploring the behavior of step size and mini-batch size for a large number of models and datasets.

2 Revisiting Hamiltonian SDE for sampling

Summary: In this section precise convergence rates conditions for generic class of integrators are presented. We suggest moreover to consider the symplectic nature of the underlying geometries as a fundamental property to be preserved.

Given a dataset of observations $D = \{\mathbf{x}_i\}_{i=1}^N$, the Bayesian treatment of machine learning models can be summarized as the combination of a prior belief $p(\boldsymbol{\theta})$ and a likelihood function $p(D|\boldsymbol{\theta})$, into a posterior distribution $p(\boldsymbol{\theta}|D) \propto p(D|\boldsymbol{\theta})p(\boldsymbol{\theta})$. Since the posterior is analytically intractable for non-linear models such as BNNs [6], our goal is to draw samples from the density $p(\boldsymbol{\theta}|D)$, which is

¹Here for simplicity we consider $C \in \mathbb{R}$, but in general C can be a matrix.

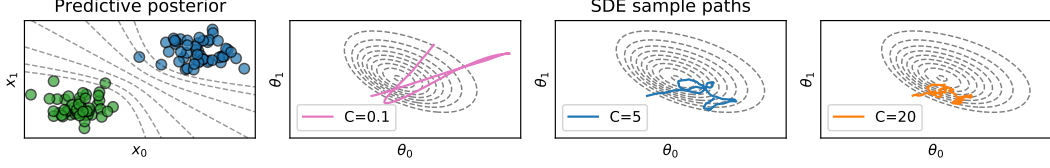


Figure 1: Sample paths for simple a two-parameter logistic regression problem. We show SDE paths for different choices of friction coefficient C .

expressed implicitly in exponential form as $p(\boldsymbol{\theta}|\mathcal{D}) \propto \exp(-U(\boldsymbol{\theta}))$, where:

$$-U(\boldsymbol{\theta}) = \sum_{i=1}^N \log p(\mathbf{x}_i|\boldsymbol{\theta}) + \log p(\boldsymbol{\theta}), \quad \text{and} \quad p(\mathcal{D}|\boldsymbol{\theta}) = \prod_{i=1}^N p(\mathbf{x}_i|\boldsymbol{\theta}). \quad (2)$$

In the context of Hamiltonian-based methods, $U(\boldsymbol{\theta})$ is known as the *potential*, which, together with a *kinetic energy* term, yields the Hamiltonian function $H(\mathbf{z}) = U(\boldsymbol{\theta}) + 1/2 \|\mathbf{M}^{-1}\mathbf{r}\|^2$. The vector $\mathbf{z} = [\mathbf{r}^\top, \boldsymbol{\theta}^\top]^\top$ denotes the overall system state, which includes the position $\boldsymbol{\theta}$ (i.e., parameters) and the conjugate momentum \mathbf{r} , while \mathbf{M} is a symmetric, positive definite mass matrix. Then we consider the following SDE, which is a compact form of Eq. (1):

$$d\mathbf{z}(t) = \begin{bmatrix} -C\mathbf{I} & -\mathbf{I} \\ \mathbf{I} & \mathbf{0} \end{bmatrix} \nabla H(\mathbf{z}(t))dt + \begin{bmatrix} \sqrt{2C}d\mathbf{w}(t) \\ \mathbf{0} \end{bmatrix}. \quad (3)$$

We study the stationary behavior of the process of Eq. (3), defining $\nabla \mathbf{z} = [\nabla \mathbf{r}^\top, \nabla \boldsymbol{\theta}^\top]^\top$, through the following differential operator:

$$\mathcal{L} = -(\nabla_{\boldsymbol{\theta}}^\top U(\boldsymbol{\theta})) \nabla_{\mathbf{r}} + \left((\mathbf{M}^{-1}\mathbf{r})^\top \right) \nabla_{\boldsymbol{\theta}} - C \left((\mathbf{M}^{-1}\mathbf{r})^\top \right) \nabla_{\mathbf{r}} + C \nabla_{\mathbf{r}}^\top \nabla_{\mathbf{r}}, \quad (4)$$

which is known as the *infinitesimal generator*. The Fokker Planck equation, that can be used to obtain the stationary distribution $\rho_{ss}(\mathbf{z})$ of the stochastic process writes as $\mathcal{L}^\dagger \rho_{ss} = 0$, where † indicates the adjoint of the operator. Then we have the following theorem:

Theorem 1. *For an ergodic stochastic process described by the SDE of Eq. (3) with stationary distribution $\rho_{ss}(\boldsymbol{\theta})$ we have:*

$$\rho_{ss}(\boldsymbol{\theta}) \propto \exp(-U(\boldsymbol{\theta})) \quad (5)$$

The proof can be found in Appendix B.2. A direct implication is that simulating the stochastic process allows us to draw samples from the desired posterior. This property can be exploited to compute Bayesian averages of generic functions of interest $\phi(\boldsymbol{\theta})$ (details in Appendix B) as follows: $\int \phi(\boldsymbol{\theta})p(\boldsymbol{\theta}|\mathcal{D})d\boldsymbol{\theta} = \int \phi(\boldsymbol{\theta})\rho_{ss}(\boldsymbol{\theta})d\boldsymbol{\theta}$.

We shall refer to our scheme as SDE-based HMC (SHMC), which we note that it differs from SGHMC. In the latter, the SDE of Eq. (3) is modified so that it has covariance matrix $2(C - \tilde{\mathbf{V}})$, where $\tilde{\mathbf{V}}$ is an estimate of the covariance of the gradient. This was done to counterbalance the effect of the stochastic gradient, which we believe is not necessary, as we discuss in Section 5. To conclude, the friction term C , as well as the diffusion term $2C$, are simply necessary to ensure that the SDE has stationary distribution $\rho_{ss}(\boldsymbol{\theta})$ that corresponds to the posterior of interest $p(\boldsymbol{\theta}|\mathcal{D})$.

Some sample paths for a simple two-parameter logistic regression can be seen in Fig. 1, where we vary the constant C . Although the stationary distribution is independent of C , the transient dynamics change, which might have an effect on practical applications. In Section 5 we explore experimentally the effect of C on a wide range machine learning models.

In recent literature, Eq. (3) has been associated with normally-distributed estimates of the gradient [10; 33]. In our view, however, this connection is not well-justified, as for the Brownian motion term of Eq. (3) we have that $d\mathbf{w}(t) = \sqrt{dt}\mathcal{N}(\mathbf{0}, \mathbf{I})$, while a (Gaussian) stochastic gradient term in the continuous limit becomes $dt\mathcal{N}(\mathbf{0}, \mathbf{I})$. A more detailed exposition can be found in Appendix A. Our alternative treatment for the study of the effect of mini-batches follows in Section 3.

2.1 Ergodic errors of SDEs

Except from a handful of cases, it is not possible to draw exact sample paths from arbitrary SDEs. We consider a generic numerical integrator ψ , with step size η , whose purpose is to simulate the stochastic evolution of the SDE of interest. Formally, we look for a stochastic mapping, that from a given initial condition \mathbf{z}_0 , generates a new random variable $\mathbf{z}_1 = \psi(\mathbf{z}_0; \eta)$ by faithfully simulating the true continuous time stochastic dynamics $\mathbf{z}(\eta)|_{\mathbf{z}(0)=\mathbf{z}_0}$. Several quantitative metrics measuring the degree of accuracy of the simulation are available [27]. The simplest is the strong error, which is the expected difference between true paths and simulated ones. Relaxing to the expected difference between functions of paths corresponds to quantifying the weak error:

Definition 1. [14] Consider Eq. (3) with initial condition \mathbf{z}_0 . The numerical integrator ψ has weak order of convergence p if $|\mathbb{E}[\phi(\psi(\mathbf{z}_0; \eta))] - \mathbb{E}[\phi(\mathbf{z}(\eta))]| = \mathcal{O}(\eta^{p+1})$, where $\mathbf{z}(\eta)$ is the value taken by Eq. (3) after a time η , the chosen step size.

The transformation of the functions ϕ of the true stochastic dynamics $\mathbf{z}(t)$, starting from initial conditions \mathbf{z}_0 is described by the Kolmogorov differential equation $\mathbb{E}[\phi(\mathbf{z}(t))] = \exp(t\mathcal{L})\phi(\mathbf{z})|_{\mathbf{z}=\mathbf{z}_0}$, that throughout the paper we indicate with abuse of notation as $\mathbb{E}[\phi(\mathbf{z}(t))] = \exp(t\mathcal{L})\phi(\mathbf{z}_0)$. The operator \mathcal{U} , defined as $\mathcal{U}\phi(\mathbf{z}_0) = \mathbb{E}[\phi(\psi(\mathbf{z}_0; \eta))]$, represents a p th order weak integrator if $\mathcal{U} = \exp(\eta\mathcal{L}) + \mathcal{O}(\eta^{p+1})$.

Since we are only interested in samples from $p(\theta|\mathcal{D})$, it is sufficient to consider the even weaker *ergodic average error*, defined hereafter. The numerical integrator iteratively induces a stochastic process $\mathbf{z}_i = \psi(\mathbf{z}_{i-1}; \eta)$, $i = 1, \dots, N$. The ergodic average of a given function $\phi(\cdot)$ converges to the integral $\int \phi(\mathbf{z})\rho_{ss}^\psi(\mathbf{z})d\mathbf{z}$, where ρ_{ss}^ψ is the stationary distribution of the stochastic process induced by the numerical integrator ψ . The ergodic average error is the difference between the ergodic average of the numerical integrator and the true average obtained with the stationary distribution of Eq. (3):

$$e(\psi, \phi) = \int \phi(\mathbf{z})\rho_{ss}^\psi(\mathbf{z})d\mathbf{z} - \int \phi(\mathbf{z})\rho_{ss}(\mathbf{z})d\mathbf{z}. \quad (6)$$

Our goal is to characterize the rate of convergence to zero of $e(\psi, \phi)$ as a function of the step size η , the most important free parameter. For the purpose of understanding the contributions of this paper, the Proposition 2, which leverages the results of [1], is sufficient. The formal statement is presented in Appendix B.3, along with a detailed technical analysis. Importantly, a sufficient condition for an integrator to be of a given ergodic order p , i.e. $e(\psi, \phi) = \mathcal{O}(\eta^p)$, is to have weak order p .

2.2 Symplectic structure

Hamiltonian systems evolve on manifolds with peculiar geometrical properties whose study is the subject of *symplectic geometry*. In the context of numerical simulations, it is a known fact that integrators that preserve the underlying geometry (a.k.a. symplectic structure) perform better than generic ones [37; 36]. Symplectic [37] and quasi symplectic [36; 1; 7] SDEs have been studied in the past, albeit in a different context than Bayesian sampling. Recently, symplectic geometry has been revisited, to characterize generic optimization problems [5; 17; 16], whereas in this work we are interested only on sampling properties.

It is possible to show (Appendix B.4) that the stochastic evolution induced by the SDE in Eq. (3), starting from generic initial conditions $\mathbf{z}(0)$, $\mathbf{z}(t) = \tau(\mathbf{z}(0))$, dissipates the volume of regions exponentially fast. In precise mathematical terms, the evolution has Jacobian $\Omega_{m,n} = \frac{\partial \tau_m(z)}{\partial z_n}$ that satisfies $\det(\Omega) = \exp(-C\text{Tr}(\mathbf{M}^{-1})t)$. The underlying geometry is in many aspects related to the one of symplectic manifolds, where volume is preserved exactly. It is natural to expect that numerical integrators that almost preserve the symplectic structure, defined as quasi-symplectic, when applied to systems as Eq. (3), will perform better than generic integrators. An excellent exposition of the details of such statement is presented in [37; 36; 35].

2.3 Numerical integrators

We explore the effect of a number of SDE integrators of weak order two; these schemes are outlined in detail in Appendix B.5. For stochastic systems with additive noise, the direct extension of a two-stage Runge-Kutta (RK2) scheme is provably of second order [27]; however, it is not quasi-symplectic.

The LEAPFROG scheme is probably the simplest form of quasi-symplectic integrator, which involves updating the position and momentum at interleaved time steps. Importantly, while it has theoretically order-one of convergence both in weak and ergodic sense, we observe empirically that its performance is indistinguishable from other symplectic order-two schemes. A similar phenomenon has been observed in [36]. Although what we present is not a proof, in Appendix E.2 we discuss the Taylor expansion of the operator induced by the scheme, providing insights about its performance. We leave further explorations for future work.

In the experimental section, we also examine the symmetric splitting integrator proposed in [9] (SYMMETRIC), which is also compatible with our SHMC scheme. Finally we consider a LIE-TROTTER splitting scheme [2] that is of weak order-two, while it is also quasi-symplectic. In Section 4 this scheme will be used to draw a theoretical connection between HMC [40] and the proposed SDE framework in Eq. (3).

3 Minibatches as operator splitting

Contribution: the effect of mini-batching can be understood through the purely geometrical perspective of differential operator splitting, without the need for any central limit theorem assumption on the statistics of the SG noise. The net effect can be precisely quantified in the form of convergence rates.

Traditionally, the effect of mini-batching has been modeled as a source of additional independent Gaussian noise [10] at every step of the simulated dynamics. We challenge this common modeling assumption by considering the geometrical perspective of differential operator splitting. We build the link between the true generator \mathcal{L} and numerical integration performed using mini-batch subsets of the full potential. Importantly our analysis does not make any assumption about Gaussianity of SG noise.

Our approach is rooted in the geometrical view of splitting schemes for high dimensional Hamiltonian systems [13],[45],[22],[12],[31].

This allows us to derive Theorem 3, which presents a result in terms of convergence rate to the desired posterior distribution. A purely geometrical approach has not received much attention in the context of data subsampling for Bayesian inference, with the notable exceptions of [4; 42] that explored related ideas for the case of HMC only.

Without loss of generality, suppose that the dataset D is split into two mini-batches D_1, D_2 . Following Eq. (4) we can define the infinitesimal generators $\mathcal{L}_1, \mathcal{L}_2$, for which we have $\mathcal{L} = \mathcal{L}_1 + \mathcal{L}_2$. Intuitively, given an operator in exponential form $\exp(\eta(\mathcal{L}_1 + \mathcal{L}_2))$, we would like to determine under which conditions the following holds

$$\exp(\eta(\mathcal{L}_1 + \mathcal{L}_2)) \simeq \exp(\eta\mathcal{L}_1) \exp(\eta\mathcal{L}_2), \quad (7)$$

and more importantly, quantify the discrepancy error in a rigorous way. In the general case we consider splittings into K mini-batches of the form $\mathcal{L} = \sum_{i=1}^K \mathcal{L}_i$ where

$$\mathcal{L}_i = -(\nabla_{\theta}^{\top} U_i(\theta)) \nabla_{\mathbf{r}} + K^{-1} \left((\mathbf{M}^{-1} \mathbf{r})^{\top} \right) \nabla_{\theta} - K^{-1} C \left((\mathbf{M}^{-1} \mathbf{r})^{\top} \right) \nabla_{\mathbf{r}} + K^{-1} C \nabla_{\mathbf{r}}^{\top} \nabla_{\mathbf{r}}, \quad (8)$$

with $U_i(\theta)$ the potential computed using only the i_{th} mini-batch. The theorems presented in this section clarify how concatenations of the form $\prod_i \exp(\eta\mathcal{L}_i)$ induce errors and clarify their relevance for the considered problem.

The following theorem characterizes the order of convergence of the randomized splitting scheme.

Theorem 2. *Consider a class of numerical integrators with order p . Split the full dataset into K mini-batches and consider numerical integrators ψ_i of order p obtained using the mini-batches, i.e. $\mathbb{E}[\phi_i(\psi(\mathbf{z}_0; \eta))] = \exp(\eta\mathcal{L}_i)\phi(\mathbf{z}_0) + \mathcal{O}(\eta^{p+1})$. Extract uniformly $\boldsymbol{\pi} = [\pi_1, \dots, \pi_K] \in \mathbb{P}$, the set of all the possible permutations of the indices $\{1, K\}$. The scheme in which initial condition has stochastic evolution through the chain of integrators with order*

$$\mathbf{z}_{\text{fin}} = \psi_{\pi_K}(\psi_{\pi_{K-1}}(\dots \psi_{\pi_1}(\mathbf{z}_0))), \quad (9)$$

transforms the functions ϕ with an operator \mathcal{U} that has the following expression

$$\mathcal{U} = \exp(\eta\mathcal{L}) + \mathcal{O}(K\eta^{\min(p+1,3)}) \quad (10)$$

The proof can be found in Appendix C.4. Particularly relevant to our discussion are works that explore randomized splitting schemes for Hamiltonian simulation, but not in a sampling context [11; 54].

Intuitively, this means that if we pick a random permutation of the batches and apply the sequence of numerical integrators accordingly, we induce an operator that transforms functions ϕ with an error that has order $\mathcal{O}(K\eta^{\min(p+1,3)})$. Theorem 2 allows to state Theorem 3, which is a central result of this discussion.

Theorem 3. *Consider the settings described by Theorem 2. Repeatedly apply the numerical integration scheme. Then the ergodic error has expansion*

$$e(\psi, \phi) = \mathcal{O}(K\eta^{\min(p,2)}) \quad (11)$$

See Appendix C.5 for the proof. This theorem tells us that the net effect of mini-batches is an extra error of order two in the convergence rate. Importantly, this error can become the bottleneck whenever $p > 2$. This extra error is not due to an equivalent noise injection into the SDE dynamics, and attempting to counterbalance it, as suggested by the literature [10], is irrelevant as we will show in Section 5. Although in this work we focus on the ergodic behavior, non asymptotic convergence rates are studied in [9]; see Appendix F for a detailed discussion.

Details on the constants in the convergence results

Some clarifications are in order. First, the constant K , the number of mini-batches, appearing in the \mathcal{O} notation could be refined considering the geometry of the potentials. We leave such a possibility for future works and refer the interested reader to [13; 11] and in particular also to [54], that proposes randomized schemes strictly related to the one discussed here. Second, when performing Bayesian sampling, the full potential is divided into mini-batches, and each subset rescaled by the constant K . This corresponds to modifying the infinitesimal generator as follows: $\mathcal{L} \rightarrow K\mathcal{L} = \sum_i (K\mathcal{L}_i)$. The resulting strategy allows one to “cover” the same amount of distance per steps independently from K , given that in the original formulation one would need K steps to simulate $\exp(\eta\mathcal{L})$. Importantly, the desired stationary distribution is the same since $\mathcal{L}^\dagger \rho_{ss} = 0 \iff (K\mathcal{L})^\dagger \rho_{ss} = 0$. Equivalently, the procedure corresponds to the simulation of the original system with step size $\eta \rightarrow K\eta$. This immediately translates into larger constants in Theorem 3 and Theorem 2. For the case of HMC, this is acknowledged in [4], drawing an equivalence with the work of [42], with new step size $K\eta$.

4 Connections with HMC in the language of operators

Contribution: we show that HMC can be interpreted as a LIE-TROTTER scheme. We provide insights, also in terms of convergence rates, of the superior performance of SHMC schemes and consequently recommend their usage instead of HMC.

We shall draw a connection between Hamiltonian SDEs and the original HMC algorithm, by showing that the latter can be interpreted as an integration scheme of the SDE dynamics. The infinitesimal generator Eq. (4) can be expressed as the sum of two components:

$$\mathcal{H} = -(\nabla_\theta^\top U(\theta)) \nabla_{\mathbf{r}} + \left((\mathbf{M}^{-1}\mathbf{r})^\top \right) \nabla_\theta, \quad \mathcal{D} = -C \left((\mathbf{M}^{-1}\mathbf{r})^\top \right) \nabla_{\mathbf{r}} + C \nabla_{\mathbf{r}}^\top \nabla_{\mathbf{r}}.$$

The LIE-TROTTER scheme is the starting point of our exposition. In its general form [1], it consists of alternating steps that solve the \mathcal{H} and \mathcal{D} parts of \mathcal{L} . It can be easily shown [1] that whenever the numerical integrator ψ for the Hamiltonian part \mathcal{H} has order p , the LIE-TROTTER scheme has convergence order $\mathcal{O}(\eta^p)$, since the term \mathcal{D} can be solved exactly. The aim of the remaining part of this Section is to show the connection between HMC and the LIE-TROTTER scheme.

The HMC algorithm [40] is composed of two nested loops in which a pure deterministic Hamiltonian dynamic is simulated and then momentum is resampled from a Gaussian distribution. The general algorithm we consider is HMC with partial momentum refreshment ([40], Eq. (5.19), [25]).

Proposition 1. Consider a deterministic order- p integrator ψ for the pure Hamiltonian dynamics (corresponding to operator \mathcal{H} of Eq. (4)).

The HMC algorithm with partial momentum refreshment consists of the following (repeated) steps

$$\mathbf{z}^* = [\mathbf{r}^{*\top}, \boldsymbol{\theta}^{*\top}]^\top = \underbrace{\psi(\dots\psi(\psi(\mathbf{z}_0)))}_{N_l \text{ times}}, \quad [\boldsymbol{\theta}_1^\top, \mathbf{r}_1^\top] = [\boldsymbol{\theta}^{*\top}, \alpha \mathbf{r}^{*\top} + \sqrt{1 - \alpha^2} \mathbf{w}^\top] \quad (12)$$

where $\mathbf{w} \sim \mathcal{N}(\mathbf{0}, \mathbf{I})$, $\alpha > 0$, and N_l is assumed to be finite. Then, we can interpret HMC as a variation of LIE-TROTTER splitting scheme with N_l times the ergodic error

$$e(\phi, \psi) = \mathcal{O}(N_l \eta^p). \quad (13)$$

Proof in Appendix D.1. We stress that we included the constant N_l in the convergence rate to underline that although in \mathcal{O} notation the rates are the same, we can claim that the constant is bigger than the simple LIE-TROTTER scheme. According to this analysis, our theory suggests to use the classical LIE-TROTTER ($N_l = 1$) instead of HMC, for which we have $N_l > 1$. This interesting insights further strengthen the connection between the numerical integration schemes for the dynamics in Eq. (3) and the HMC family.

The most widely adopted variation of HMC is the one with full momentum resampling. This corresponds to the aforementioned scheme in the case $\alpha = 0$, that in turns is achieved when considering $C \rightarrow \infty$. Such a limiting scenario poses some technical difficulties in providing precise convergence rates. We conjecture however that such a limiting case has at best performance matching the one of the scheme with partial momentum refreshment. Summarizing, our theory proves that LIE-TROTTER schemes outperform the corresponding HMC counterparts with partial momentum refreshment by a factor N_l in the constants of the convergence rates, and we conjecture that HMC with full momentum resampling is at best as good as the partial refreshment case, leading to the logical conclusion that LIE-TROTTER schemes outperform classical HMC. Although a full precise analysis is left for future work, the extensive experimental campaign reported in Section 5 corroborates our intuition, by clearly showing that SHMC based schemes outperform HMC.

5 Experiments

Comparison framework. The main objective of the experiments is to investigate convergence to the true posterior distribution for a wide range of BNN models and datasets. Metrics that reflect regression and classification accuracy are not of main interest; nevertheless, some of these are reported in Appendix G.1. Instead, we turn our attention to the quality of the predictive distribution.

We consider the true predictive posterior as the ground truth, which is approximated by a careful application of SGHMC [44] featuring a very small step size and full-batch gradient calculation. Any comparison between high-dimensional empirical distributions gives rise to significant challenges. Therefore, we resort to comparing one-dimensional predictive distributions by means of the Kolmogorov distance. For a given test dataset, we explore the average Kolmogorov distance from the true posterior predictive distributions for different methods, step sizes and mini-batch sizes. These should be compared with average and Kolmogorov *self-distance*, which is marked as grey dotted lines in the figures that follow². In all cases we compare empirical distributions of 200 samples; see Appendix G.2 for a complete account.

For SHMC, we examine four integrators with different properties: EULER, LEAPFROG, RK2 and LIE-TROTTER, and we investigate whether they differ from HMC and SGHMC [10]. For HMC we set the integration length (in steps) to be equal to the thinning parameter of SHMC, so that the running time is similar in all cases. However, RK2 is twice as slow as the rest of the methods, as it is the only two-stage scheme. We also compare against the symmetric splitting integrator proposed in [9], which we refer to as SYMMETRIC. For all cases except HMC, we set $C = 5$; we find this to be a reasonable choice (see Appendix G.4).

We consider four regression datasets (BOSTON, CONCRETE, ENERGY, YACHT) and two classification datasets (IONOSPHERE, VEHICLE) from the UCI repository, as well as a 1-D synthetic dataset, for which the regression result is shown in Appendix G.1. Due to space limitations, here we only present

²This emulates the famous Kolmogorov-Smirnov test, but with no Gaussianity assumptions

the results for BOSTON. The rest of the results can be found in Appendix G.3 and Appendix G.4. In what follows, we summarize some findings that apply to all the datasets and models we have considered.

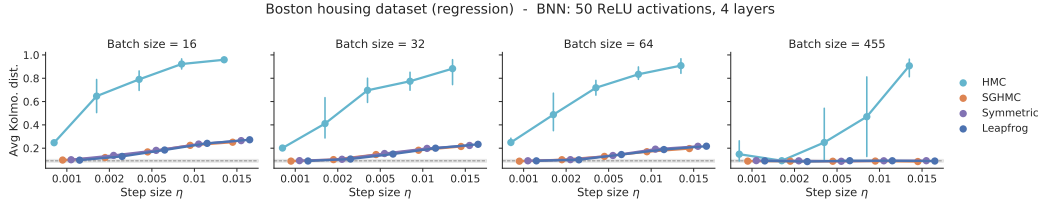


Figure 2: Exploration of step size and batch size for different Hamiltonian-based methods; the grey dotted line denotes the self-distance for the distribution of the oracle. The standard HMC cannot compete with SDE-based methods given the computational budget, as careful tuning of the integration length is required. The rest of the methods have similar behavior; the noise counterbalancing of SGHMC does not seem to offer any improvement regarding the posterior approximation over SHMC with LEAPFROG.

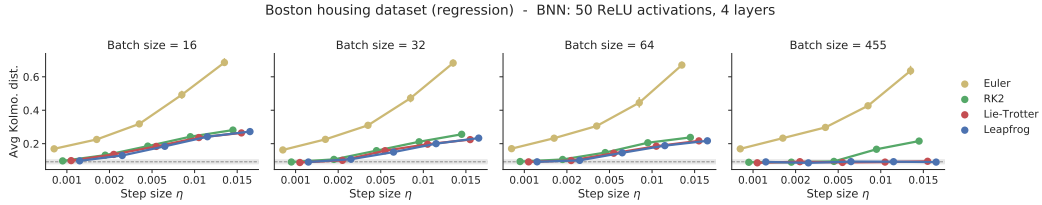


Figure 3: Exploration of step size and batch size for different SHMC integrators; the grey dotted line denotes the self-distance for the distribution of the oracle. Notice that LEAPFROG behaves as a second order integrator, although it is provably only of order-1.

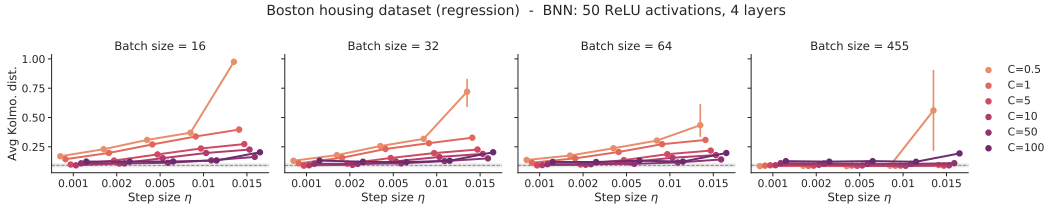


Figure 4: Exploration of step size and batch size for different values of a scalar friction coefficient C . The grey dotted line denotes the self-distance for the distribution of the oracle. The LEAPFROG integrator is used in all cases.

The effect of mini-batches. All experimental results (Fig. 2–Fig. 4) are in line with the theoretical findings which predict convergence to the true posterior of order $\mathcal{O}(\eta^2)$ for order-two integrators. We see that in all cases the posterior is well-approximated as the step size η approaches zero. Also, the size of mini-batches does have a visible effect on convergence. For larger mini-batch sizes (or equivalently, for smaller gradient noise) the model can admit larger step sizes.

Notes on SHMC. In Fig. 2 we compare SHMC (LEAPFROG integrator) with methods from the literature, including HMC, SGHMC [10] and SYMMETRIC [9]. We note that SHMC (LEAPFROG) is different from SGHMC in the sense that no counterbalancing of the noise is performed. Nevertheless, we do not observe significant difference among LEAPFROG, SGHMC and SYMMETRIC. We argue that this result is compatible with our position that counterbalancing the gradient noise is not necessary to sample from the posterior.

Notes on HMC. Regarding the behavior of HMC, we see that it seems to converge the true posterior in some cases only (i.e. BOSTON here, IONOSPHERE and VEHICLE in the appendix). We can also see, however, that the curve of HMC raises significantly faster than the other methods as the step

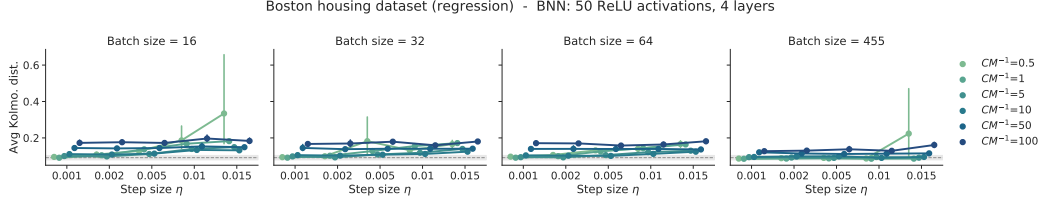


Figure 5: Exploration of step size and batch size for different values of the product CM^{-1} , where we set $M = \tilde{V}$. The grey dotted line denotes the self-distance for the distribution of the oracle. The LEAPFROG integrator is used in all cases.

size grows. We stress that that HMC has been given exactly the same computational budget and hyperparameters (step size, integration length) as the other methods in this comparison. Although it is possible to obtain better results by careful tuning [40; 23], our priority has been to demonstrate the difference in convergence, reflecting our theoretical discussion in Section 4.

Comparison of integrators. In Fig. 3, although all of the integrators considered converge to the true posterior regardless of the mini-batch size given a sufficiently small step size, we observe that the methods behave differently depending on their theoretical properties. As expected, the EULER integrator exhibits the worst behavior in terms of convergence, as it is only of order $\mathcal{O}(\eta)$. The two-stage RK2 scheme converges for significantly larger η values, which is an expected result given the order of $\mathcal{O}(\eta^2)$. It is important to note that LEAPFROG and LIE-TROTTER, which are symplectic schemes, exhibit even more attractive properties (RK2 appears to be less stable for the majority of datasets in Appendix G.3). The benefits of symplectic integrators are very well-known in the literature, and our results are in line with this common knowledge.

The effect of C . Although the SDE of Eq. (1) is guaranteed to converge to the posterior distribution for any choice of C , its transient properties are affected, which might have implications on a practical level. We investigate experimentally a fairly wide range of values for scalar C . The results of Fig. 4 imply that for the range between 5 and 10 the simulated SDE is rather robust to the choice of C . A more detailed account can be found in Appendix G.4.

Preconditioning. Finally, we explore a scheme for adapting the friction matrix based on the variability of the gradient during a pre-simulation phase, as proposed in [44], but without counterbalancing the gradient noise. In this case, instead of a scalar C , we have a diagonal matrix \mathbf{C} , which is implicitly defined through the mass matrix \mathbf{M} and the scalar constant $c_{\mathbf{M}} = \mathbf{C}\mathbf{M}^{-1}$. The scheme constitutes a kind of preconditioning, as the gradient components with high variability will be associated with smaller step sizes. The results of exploring the scalar $c_{\mathbf{M}}$ can be found in Fig. 5, as well as in Appendix G.5. In general, this parameterization is more robust compared to a scalar choice for C ; we argue that this is a sensible strategy to automatically tune the SDE parameters, and the experimental results provide further support to this position.

6 Conclusions

We have reviewed the problem of sampling from a Bayesian posterior distribution by means of simulating a Hamiltonian SDE. We have considered an extension of the dynamics of the HMC algorithm with a friction term and an appropriately scaled Brownian motion. Although this construct has appeared before in the literature [10], we have performed a novel theoretical analysis that exposes the convergence properties of Hamiltonian-based SDEs as sampling methods.

In previous works, the stochastic component of the SDE has been associated with stochastic gradient estimates. However, we have argued that the Brownian motion is a poor model of this kind of gradient noise, as the two terms scale differently with the step size. The combination of the Brownian motion with the friction term are simply necessary in order to design an SDE that features the desired stationary behavior. Instead, we have investigated the effect of gradient noise that is due to data subsampling in the context of differential operator splitting. This has allowed us to produce new convergence results for Hamiltonian SDE-based sampling methods, as well as to draw a theoretical connection to the original HMC algorithm.

We have found that for a selection of integrators of weak order two, both the discretization and the mini-batch error vanish at rate $\mathcal{O}(\eta^2)$, for integrator step size η . From a practical perspective, we recommend a straightforward simulation of the SDE in Eq. (1) by means of a symplectic second order integrator. We have demonstrated this convergence on a wide range of experiments, where we have meticulously documented the deviation from the true posterior distribution.

As a final remark, SHMC with mini-batches can be easily applied to more complex models and larger datasets, however, our experimental analysis could not be trivially scaled to deeper architectures. Despite the difficulties of reasoning about the true posterior distribution of deep BNNS, we think that an extension of our analysis to deep BNNS is a promising direction for future work.

Acknowledgement

Maurizio Filippone gratefully acknowledges support from the AXA Research Fund and the Agence Nationale de la Recherche (grant ANR-18-CE46-0002).

References

- [1] A. Abdule, G. Vilmart, and K. C. Zygalakis. High order numerical approximation of the invariant measure of ergodic sdes. *SIAM Journal on Numerical Analysis*, 52(4):1600–1622, 2014.
- [2] A. Abdule, G. Vilmart, and K. C. Zygalakis. Long time accuracy of Lie-Trotter splitting methods for Langevin dynamics. *SIAM Journal on Numerical Analysis*, 53(1):1–16, 2015.
- [3] S. Ahn, A. Korattikara, and M. Welling. Bayesian posterior sampling via stochastic gradient Fisher scoring. In *International Conference on Machine Learning*, pages 1771–1778, 2012.
- [4] M. Betancourt. The fundamental incompatibility of scalable Hamiltonian Monte Carlo and naive data subsampling. In F. Bach and D. Blei, editors, *International Conference on Machine Learning*, volume 37 of *Proceedings of Machine Learning Research*, pages 533–540, Lille, France, 07–09 Jul 2015.
- [5] M. Betancourt, M. I. Jordan, and A. C. Wilson. On symplectic optimization. *arXiv preprint arXiv:1802.03653*, 2018.
- [6] C. M. Bishop. *Pattern recognition and machine learning*. Springer, 1st ed. 2006. corr. 2nd printing 2011 edition, 2006.
- [7] N. Bou-Rabee and H. Owhadi. Long-run accuracy of variational integrators in the stochastic context. *SIAM Journal on Numerical Analysis*, 48(1):278–297, 2010.
- [8] P. Chaudhari and S. Soatto. Stochastic gradient descent performs variational inference, converges to limit cycles for deep networks. In *2018 Information Theory and Applications Workshop (ITA)*, pages 1–10. IEEE, 2018.
- [9] C. Chen, N. Ding, and L. Carin. On the convergence of stochastic gradient MCMC algorithms with high-order integrators. *Advances in neural information processing systems*, 28:2278–2286, 2015.
- [10] T. Chen, E. Fox, and C. Guestrin. Stochastic gradient Hamiltonian Monte Carlo. In *International conference on machine learning*, pages 1683–1691, 2014.
- [11] A. M. Childs, A. Ostrander, and Y. Su. Faster quantum simulation by randomization. *Quantum*, 3:182, 2019.
- [12] A. M. Childs and Y. Su. Nearly optimal lattice simulation by product formulas. *Physical review letters*, 123(5):050503, 2019.
- [13] A. M. Childs, Y. Su, M. C. Tran, N. Wiebe, and S. Zhu. Theory of Trotter error with commutator scaling. *Physical Review X*, 11(1):011020, 2021.

- [14] A. Debussche and E. Faou. Weak backward error analysis for sdes. *SIAM Journal on Numerical Analysis*, 50(3):1735–1752, 2012.
- [15] E. B. Dynkin. Calculation of the coefficients in the campbell-hausdorff formula. In *Dokl. Akad. Nauk. SSSR (NS)*, volume 57, pages 323–326, 1947.
- [16] G. França, M. I. Jordan, and R. Vidal. On dissipative symplectic integration with applications to gradient-based optimization. *Journal of Statistical Mechanics: Theory and Experiment*, 2021(4):043402, 2021.
- [17] G. França, J. Sulam, D. P. Robinson, and R. Vidal. Conformal symplectic and relativistic optimization. *Journal of Statistical Mechanics: Theory and Experiment*, 2020(12):124008, 2020.
- [18] F. Futami, I. Sato, and M. Sugiyama. Accelerating the diffusion-based ensemble sampling by non-reversible dynamics. In *International Conference on Machine Learning*, pages 3337–3347, 2020.
- [19] X. Gao, M. Gurbuzbalaban, and L. Zhu. Breaking reversibility accelerates Langevin dynamics for global non-convex optimization. *arXiv preprint arXiv:1812.07725*, 2018.
- [20] X. Gao, M. Gürbüzbalaban, and L. Zhu. Global convergence of stochastic gradient Hamiltonian Monte Carlo for non-convex stochastic optimization: Non-asymptotic performance bounds and momentum-based acceleration. *arXiv preprint arXiv:1809.04618*, 2018.
- [21] C. W. Gardiner. *Handbook of stochastic methods for physics, chemistry and the natural sciences*, volume 13 of *Springer Series in Synergetics*. Springer-Verlag, third edition, 2004.
- [22] N. Hatano and M. Suzuki. Finding exponential product formulas of higher orders. In *Quantum annealing and other optimization methods*, pages 37–68. Springer, 2005.
- [23] M. D. Hoffman and A. Gelman. The no-u-turn sampler: Adaptively setting path lengths in Hamiltonian Monte Carlo. *J. Mach. Learn. Res.*, 15(1):1593–1623, Jan. 2014.
- [24] L. Hörmander. Hypoelliptic second order differential equations. *Acta Mathematica*, 119(1):147–171, 1967.
- [25] A. M. Horowitz. A generalized guided Monte Carlo algorithm. *Physics Letters B*, 268(2):247–252, 1991.
- [26] A. Jacot, F. Gabriel, and C. Hongler. Neural Tangent Kernel: Convergence and Generalization in Neural Networks. In *Advances in Neural Information Processing Systems*, volume 31, pages 8571–8580. Curran Associates, Inc., 2018.
- [27] P. E. Kloeden and E. Platen. *Numerical solution of stochastic differential equations*, volume 23. Springer Science & Business Media, 2013.
- [28] J. Lee, S. S. Schoenholz, J. Pennington, B. Adlam, L. Xiao, R. Novak, and J. Sohl-Dickstein. Finite versus infinite neural networks: an empirical study. In *Advances in Neural Information Processing Systems*, volume 33 (to appear), 2020.
- [29] T. Leen and J. Moody. Weight space probability densities in stochastic learning: I. dynamics and equilibria. *Advances in neural information processing systems*, 5:451–458, 1992.
- [30] X. Li, Y. Wu, L. Mackey, and M. A. Erdogdu. Stochastic Runge-Kutta accelerates Langevin Monte Carlo and beyond. In *Advances in Neural Information Processing Systems*, pages 7748–7760, 2019.
- [31] G. H. Low, V. Kliuchnikov, and N. Wiebe. Well-conditioned multiproduct Hamiltonian simulation. *arXiv preprint arXiv:1907.11679*, 2019.
- [32] Y.-A. Ma, T. Chen, and E. Fox. A complete recipe for stochastic gradient mcmc. In *Advances in Neural Information Processing Systems*, pages 2917–2925, 2015.

- [33] S. Mandt, M. D. Hoffman, and D. M. Blei. Stochastic gradient descent as approximate Bayesian inference. *The Journal of Machine Learning Research*, 18(1):4873–4907, 2017.
- [34] J. C. Mattingly, A. M. Stuart, and M. V. Tretyakov. Convergence of numerical time-averaging and stationary measures via poisson equations. *SIAM Journal on Numerical Analysis*, 48(2):552–577, 2010.
- [35] G. Milstein and M. Tretyakov. Computing ergodic limits for Langevin equations. *Physica D: Nonlinear Phenomena*, 229(1):81–95, 2007.
- [36] G. Milstein and M. V. Tretyakov. Quasi-symplectic methods for Langevin-type equations. *IMA journal of numerical analysis*, 23(4):593–626, 2003.
- [37] G. N. Milstein, Y. M. Repin, and M. V. Tretyakov. Symplectic integration of Hamiltonian systems with additive noise. *SIAM Journal on Numerical Analysis*, 39(6):2066–2088, 2002.
- [38] J. Mukhoti, P. Stenertorp, and Y. Gal. On the importance of strong baselines in Bayesian deep learning. In *NeurIPS 2018: Workshop on Bayesian Deep Learning*, 2018.
- [39] R. M. Neal. *Bayesian Learning for Neural Networks (Lecture Notes in Statistics)*. Springer, 1996.
- [40] R. M. Neal et al. Mcmc using Hamiltonian dynamics. *Handbook of Markov chain Monte Carlo*, 2(11):2, 2011.
- [41] S. Patterson and Y. W. Teh. Stochastic gradient Riemannian Langevin dynamics on the probability simplex. In C. J. C. Burges, L. Bottou, M. Welling, Z. Ghahramani, and K. Q. Weinberger, editors, *Advances in Neural Information Processing Systems*, pages 3102–3110. Curran Associates, Inc., 2013.
- [42] B. Shahbaba, S. Lan, W. O. Johnson, and R. M. Neal. Split Hamiltonian Monte Carlo. *Statistics and Computing*, 24(3):339–349, 2014.
- [43] B. Shi, W. J. Su, and M. I. Jordan. On learning rates and schrödinger operators. *arXiv preprint arXiv:2004.06977*, 2020.
- [44] J. T. Springenberg, A. Klein, S. Falkner, and F. Hutter. Bayesian optimization with robust Bayesian neural networks. In *Advances in neural information processing systems*, pages 4134–4142, 2016.
- [45] M. Suzuki. On the convergence of exponential operators—the Zassenhaus formula, BCH formula and systematic approximants. *Communications in Mathematical Physics*, 57(3):193–200, 1977.
- [46] D. Talay. Stochastic Hamiltonian systems: exponential convergence to the invariant measure, and discretization by the implicit Euler scheme. *Markov Process. Related Fields*, 8(2):163–198, 2002.
- [47] D. Talay and L. Tubaro. Expansion of the global error for numerical schemes solving stochastic differential equations. *Stochastic analysis and applications*, 8(4):483–509, 1990.
- [48] B.-H. Tran, S. Rossi, D. Milios, and M. Filippone. All you need is a good functional prior for Bayesian deep learning, 2020.
- [49] S. J. Vollmer, K. C. Zygalakis, and Y. W. Teh. Exploration of the (non-) asymptotic bias and variance of stochastic gradient Langevin dynamics. *The Journal of Machine Learning Research*, 17(1):5504–5548, 2016.
- [50] M. Welling and Y. W. Teh. Bayesian learning via stochastic gradient Langevin dynamics. In *International Conference on Machine Learning*, pages 681–688, 2011.
- [51] F. Wenzel, K. Roth, B. Veeling, J. Swiatkowski, L. Tran, S. Mandt, J. Snoek, T. Salimans, R. Jenatton, and S. Nowozin. How good is the Bayes posterior in deep neural networks really? In *International Conference on Machine Learning*, pages 10248–10259, 2020.

- [52] P. Xu, J. Chen, D. Zou, and Q. Gu. Global convergence of Langevin dynamics based algorithms for nonconvex optimization. In *Advances in Neural Information Processing Systems*, pages 3122–3133, 2018.
- [53] S. Yaida. Fluctuation-dissipation relations for stochastic gradient descent. In *International Conference on Learning Representations*, 2019.
- [54] C. Zhang. Randomized algorithms for Hamiltonian simulation. In *Monte Carlo and Quasi-Monte Carlo Methods 2010*, pages 709–719. Springer, 2012.

A Limitations of current SDE approaches to analyze SG-based algorithms

In this Section, we expose a limitation of the literature on SDE modeling of stochastic gradient-based sampling and optimization algorithms, which in our view is contributing to foster an imprecise understanding and use of such algorithms, as we discuss in the main paper. A common approach to analyze the errors introduced by the mini-batching is to take the limit for a step size going to zero [10]. The derivations in the literature are based mainly on two assumptions: (i) the learning rate (or step size) is small enough such that transforming the discrete time update equations into continuous time ones is a valid approximation, and (ii) the mini-batch subsampling operation can be modelled, with the help of the central limit theorem, as an additional source of Gaussian noise that interferes with the dynamics. These assumptions, combined together, are used to justify the use of SDEs as models to study and analyze the dynamics of stochastic gradient-based algorithms.

According to the standard practice [10; 33], we consider the potential $U(\cdot)$, a set of parameters θ , and a minibatch gradient $\nabla \tilde{U}(\theta)$; then, by means of central limit theorem we assume:

$$\nabla \tilde{U}(\theta) = \nabla U(\theta) + \mathcal{N}(\mathbf{0}, \Sigma), \quad (14)$$

such that the discrete time dynamics of SGD becomes:

$$\begin{aligned} \delta \theta &= -\eta \nabla U(\theta) - \eta \mathcal{N}(\mathbf{0}, \Sigma), \\ &= -\eta \nabla U(\theta) - \Sigma^{1/2} \sqrt{\eta} \mathcal{N}(0, \mathbf{I}). \end{aligned} \quad (15)$$

In the limit of vanishing step size, $\eta \rightarrow dt$, we can translate the discrete time dynamics into the continuous time ones as follows:

$$d\theta = -\nabla U(\theta)dt + \Sigma^{1/2} \sqrt{\eta} d\mathbf{w}(t), \quad (16)$$

where \mathbf{w}_t is a standard Brownian motion. Loosely speaking, Brownian motion is a stochastic process whose differential satisfies $d\mathbf{w}(t) \sim \mathcal{N}(0, dt\mathbf{I})$, and whose increments are independent with respect to t . Notice that the stochastic term of Eq. (15) involves two copies of η , in the covariance $\eta\mathbf{I}$ and in the external multiplication factor $\sqrt{\eta}$, but we consider $\eta \rightarrow dt$ only for the copy that scales the covariance of the Gaussian component.

The issue with this derivation becomes apparent by considering a proper stochastic calculus perspective, where both η terms are considered as infinitesimals, yielding $\sqrt{dt}d\mathbf{w}(t) = \mathbf{0}$.

This is also explicitly noted by S. Yaida [53], where the approximation $\eta^2 \simeq \eta dt$ was criticized. Considering the true limit, it is not possible to arbitrarily decide that the same quantity can be considered both as an infinitesimal and as an arbitrarily small but finite value. The matter is not only a mathematical subtlety. If one considers the correct formulation based on Fokker-Planck equations without going into continuous time but remaining in the discrete time [29], noncentral moments of the stochastic gradients need to be considered. Crucially, these induce quantitatively and qualitatively different results for the dynamics.

Note that our work is not in contrast with the literature whose purpose is the analysis of the stochastic gradient noise [8; 43] or its approximate validity as a sampling method [33], where the formalism of SDEs is justified as a modelling tool. Our argument can be summarized as follows: if we are interested in the formal characterization of the convergence of these sampling schemes, such an assumption is invalid. When considering mini-batching in the context of sampling via SDE simulations, it is not correct to consider the stochastic gradients as an additional source of noise.

B Additional derivations for Section 2

B.1 Technical assumptions

In this Section we present the technical assumptions needed for the analysis in the paper.

We need to ensure that the Kolmogorov equation associated with the SDE Eq. (3) has regular smooth solutions and unique invariant stationary distribution independent of initial conditions. To ensure smoothness and uniqueness, it is sufficient to prove that the infinitesimal generator satisfies certain regularity conditions [24; 34], whereas to ensure ergodicity we require some growth conditions on the potential [46; 2]. Then, we need to assume that the functions $\phi(\cdot)$ satisfy certain conditions, to ensure that Taylor expansions of the form Eq. (18) are valid. Finally, we need to assume that the expected value of the considered numerical integration schemes can be validly expanded into series of the form Eq. (19).

In the following we present sufficient conditions that guarantee the validity of the aforementioned assumptions. The reader interested in relaxing such technical conditions is referred to the original sources, such as [1; 2] and the works cited therein.

The first assumption guarantees that the Kolmogorov equation has regular unique smooth solutions and that the considered SDE is ergodic.

Assumption 1. *The potential $U(\boldsymbol{\theta})$ has continuous smooth bounded derivatives of arbitrary order, and it satisfies the growth condition*

$$\boldsymbol{\theta}^\top \nabla U(\boldsymbol{\theta}) \geq R_1 \|\boldsymbol{\theta}\|^2 - R_2, \quad (17)$$

for some $R_1, R_2 > 0$

It is important to notice that these requirements are independent from considerations on the choice of integrators, and without the assumption of ergodicity none of the SDE based sampling methods are conceptually meaningful.

Next, we restrict the class of considered $\phi(\cdot)$ functions to ensure that Taylor expansions of the transformation of equation is valid.

Assumption 2. *The function $\phi(\cdot)$ belongs to the set of functions l times continuously differentiable with all the partial derivatives with polynomial growth, for some positive $l > 0$. Furthermore there exists an $s \geq 0$ such that $|\phi(\boldsymbol{\theta})| \leq R_3(1 + \|\boldsymbol{\theta}\|^s)$ for some $R_3 > 0$.*

This ensures that we can write

$$\exp(\eta \mathcal{L})\phi = \sum_{j=0}^l \frac{(\eta \mathcal{L})^j}{j!} \phi + \mathcal{O}(\eta^{l+1}), \quad (18)$$

for generic l , [47].

To be able to perform the same kind of expansions for numerical integrators, we need the following assumption.

Assumption 3. *Given an initial condition \mathbf{z}_0 , any considered numerical integrator ψ is such that*

$$|\mathbb{E}[\|\mathbf{z}_1 - \mathbf{z}_0\|]| \leq R_4(1 + \|\mathbf{z}_0\|)\eta, \quad \|\mathbf{z}_1 - \mathbf{z}_0\| \leq M_n(1 + \|\mathbf{z}_0\|)\sqrt{\eta},$$

with $\mathbf{z}_1 = \psi(\mathbf{z}_0)$, $R_4 > 0$ is independent of η , assumed small enough, and M_n has bounded moments of all orders independent of η .

This allows us to write the expansion of $\mathbb{E}[\phi(\mathbf{z}_1)|\mathbf{z}_0]$ up to generic order z as

$$\mathbb{E}[\phi(\mathbf{z}_1)|\mathbf{z}_0] = \mathcal{U}\phi = \left(\mathcal{I} + \eta \mathcal{A}_1 + \frac{\eta^2}{2} \mathcal{A}_2 + \dots \frac{\eta^z}{z!} \mathcal{A}_z + \dots \right) \phi + \mathcal{O}(\eta^{z+1}) \quad (19)$$

B.2 Proof of Theorem 1

Here prove that the stationary distribution of Eq. (3) is the posterior of interest [21]. Start from the infinitesimal generator

$$\mathcal{L} = \underbrace{-(\nabla_{\boldsymbol{\theta}}^\top U(\boldsymbol{\theta})) \nabla_{\mathbf{r}} + (\mathbf{M}^{-1} \mathbf{r})^\top \nabla_{\boldsymbol{\theta}}}_{\text{pure Hamiltonian evolution} = \mathcal{H}} - \underbrace{C (\mathbf{M}^{-1} \mathbf{r})^\top \nabla_{\mathbf{r}} + C \nabla_{\mathbf{r}}^\top \nabla_{\mathbf{r}}}_{\text{friction and Noise} = \mathcal{D}}.$$

The adjoint of the first term, the pure Hamiltonian, can be rewritten as

$$\mathcal{H}^\dagger = (\nabla_\theta^\top U(\theta)) \nabla_{\mathbf{r}} - (\mathbf{M}^{-1} \mathbf{r})^\top \nabla_\theta = \nabla_{\mathbf{z}}^\top H(\mathbf{z}) \begin{bmatrix} \mathbf{0} & -\mathbf{I} \\ \mathbf{I} & \mathbf{0} \end{bmatrix} \nabla_{\mathbf{z}} \quad (20)$$

Assuming $\rho_{ss}(\mathbf{z}) \propto \exp(-H(\mathbf{z}))$ we have

$$\begin{aligned} \mathcal{H}^\dagger \rho_{ss}(\mathbf{z}) &\propto \mathcal{H}^\dagger \exp(-H(\mathbf{z})) = \nabla_{\mathbf{z}}^\top H(\mathbf{z}) \begin{bmatrix} \mathbf{0} & -\mathbf{I} \\ \mathbf{I} & \mathbf{0} \end{bmatrix} (\nabla_{\mathbf{z}} \exp(-H(\mathbf{z}))) = \\ &= -\nabla_{\mathbf{z}}^\top H(\mathbf{z}) \begin{bmatrix} \mathbf{0} & -\mathbf{I} \\ \mathbf{I} & \mathbf{0} \end{bmatrix} \nabla_{\mathbf{z}} H(\mathbf{z}) \exp(-H(\mathbf{z})) = 0. \end{aligned}$$

Similarly, considering the adjoint of \mathcal{D}

$$\mathcal{D}^\dagger = \nabla_{\mathbf{r}}^\top (C(\mathbf{M}^{-1} \mathbf{r}) \cdot) + C \nabla_{\mathbf{r}}^\top \nabla_{\mathbf{r}} = \nabla_{\mathbf{r}}^\top (C(\mathbf{M}^{-1} \mathbf{r}) \cdot + C \nabla_{\mathbf{r}}). \quad (21)$$

We study the term

$$\begin{aligned} (C(\mathbf{M}^{-1} \mathbf{r}) \cdot + C \nabla_{\mathbf{r}}) \rho_{ss}(\mathbf{z}) &\propto \\ (C(\mathbf{M}^{-1} \mathbf{r}) \cdot + C \nabla_{\mathbf{r}}) \exp(-U(\theta) - 1/2 \|\mathbf{M}^{-1} \mathbf{r}\|^2) &= \\ \exp(-U(\theta)) (C(\mathbf{M}^{-1} \mathbf{r}) \exp(-1/2 \|\mathbf{M}^{-1} \mathbf{r}\|^2) + C \nabla_{\mathbf{r}} (\exp(-1/2 \|\mathbf{M}^{-1} \mathbf{r}\|^2))) &= \\ \exp(-U(\theta)) (C(\mathbf{M}^{-1} \mathbf{r}) \exp(-1/2 \|\mathbf{M}^{-1} \mathbf{r}\|^2) - C(\mathbf{M}^{-1} \mathbf{r}) \exp(-1/2 \|\mathbf{M}^{-1} \mathbf{r}\|^2)) &= 0. \end{aligned}$$

Consequently $\mathcal{L}^\dagger \rho_{ss} = (\mathcal{H}^\dagger + \mathcal{D}^\dagger) \rho_{ss} = 0$, concluding the proof.

B.3 Ergodic order of convergence

In this section we present the result of [2], that we use to state the order of generic schemes considered in this work.

Proposition 2. *A sufficient condition for an integrator to be of a given ergodic error p , i.e. $e(\psi, \phi) = \mathcal{O}(\eta^p)$, is to have weak order p . This is not a necessary condition, as carefully described in Theorem 4*

The following Theorem describes the generic conditions to achieve a given ergodic error.

Theorem 4. [2]. *Consider the assumptions of Section B.1. Suppose that the elements of the expansion of eq. Eq. (19) satisfy*

$$\mathcal{A}_1 = \mathcal{L}, \quad \mathcal{A}_j^\dagger \rho = 0, \quad j = 2, \dots, r. \quad (22)$$

Then the ergodic average has order of convergence r , i.e.

$$e(\psi, \phi) = \int \phi(\mathbf{z}) \rho_{ss}^\psi(\mathbf{z}) d\mathbf{z} - \int \phi(\mathbf{z}) \rho_{ss}(\mathbf{z}) d\mathbf{z} = \mathcal{O}(\eta^r). \quad (23)$$

The result can also be refined as follows:

$$e(\psi, \phi) = -\eta^r \int_0^\infty \int (\mathcal{A}_{r+1} \exp(t\mathcal{L}) \phi(\mathbf{z})) \rho(\mathbf{z}) d\mathbf{z} + \mathcal{O}(\eta^{r+1}) \quad (24)$$

The proof is presented in [2]. A similar characterization has been attempted in [9], where the requirement to achieve a given convergence rate is that the integrator has weak local error of some given order. We suggest to rely instead on the weaker requirements $\mathcal{A}_j^\dagger \rho = 0$ for $j = 1, \dots, r$. In fact, if a method has local error of order k , then, by standard backward error analysis arguments, we have that: $\mathcal{U} = \mathcal{I} + \eta \mathcal{L} + \frac{\eta^2}{2} \mathcal{L}^2 + \dots + \frac{\eta^k}{k!} \mathcal{L}^k + \mathcal{O}(\eta^{k+1})$ where we easily notice that $\mathcal{A}_j = \mathcal{L}^j$, with $j = 1, \dots, k$. Consequently $\mathcal{A}_j^\dagger \rho = 0$, for $j = 1, \dots, r$, since $\mathcal{L}^\dagger \rho = 0$ due to the Fokker Planck equation. In summary, the ergodic error order is at least the weak order of the integrator.

B.4 Quasi-symplectic integrators

We start our discussion by considering the definition of a generic *symplectic* mapping. This is an important condition, since it can be shown that the evolution of deterministic Hamiltonian ODE naturally respects this condition [16].

Definition 2. A mapping $\kappa : \mathbf{z}_0 = [\mathbf{r}_0^\top, \boldsymbol{\theta}_0^\top]^\top \rightarrow \mathbf{z}_1 = [\mathbf{r}_1^\top, \boldsymbol{\theta}_1^\top]^\top$ is said to be symplectic iff

$$\boldsymbol{\Omega}^\top \mathbf{J} \boldsymbol{\Omega} = \mathbf{J}, \quad (25)$$

where $\boldsymbol{\Omega}_{m,n} = \frac{\partial(z_1)_m}{\partial(z_0)_n}$ is the Jacobian. where $\mathbf{J} = \begin{bmatrix} \mathbf{0} & -\mathbf{I} \\ \mathbf{I} & \mathbf{0} \end{bmatrix}$.

A direct consequence of the symplectic property is that a symplectic mapping preserves the volume. Precisely, if we consider a region $O \subseteq \mathbb{R}^{2D}$, the volume after the mapping κ remains unchanged

$$\text{Vol}(\kappa(O)) = \int_O |\det(\boldsymbol{\Omega}(\mathbf{z}))| d\mathbf{z} = \int_O d\mathbf{z}, \quad (26)$$

since from Eq. (25) we easily derive, considering $\det(\boldsymbol{\Omega}^\top \mathbf{J} \boldsymbol{\Omega}) = \det(\boldsymbol{\Omega})^2$, that $\det(\boldsymbol{\Omega}) = \pm 1$.

In this work we are interested however in stochastic Hamiltonian evolutions in the form of Eq. (3). The first simple consideration we can make is that in the limit of vanishing friction, i.e. $C \rightarrow 0$, the dynamics are symplectic mappings. This is trivially derived considering that in such a limit the SDE becomes an Hamiltonian ODE and the symplectic property is proved as in [16]. When $C \neq 0$, it is possible to show that the stochastic mapping contracts exponentially in time the volume of regions. The precise statement is reported in the following Theorem.

Theorem 5. Consider an Hamiltonian SDE of the form Eq. (3) and the stochastic evolution induced by this equation starting from generic initial conditions, i.e., $\mathbf{z}(t) = \tau(\mathbf{z}(0))$. Then τ contracts the volume exponentially in time as $\det(\boldsymbol{\Omega}) = \exp(-C \text{Tr}(\mathbf{M}^{-1}) t)$, where $\boldsymbol{\Omega}_{m,n} = \frac{\partial \tau_m(z)}{\partial z_n}$ is the (random) Jacobian.

Proof. Starting from Eq. (3), we have

$$d\mathbf{z}^\top(t) = \nabla^\top H(\mathbf{z}(t)) \begin{bmatrix} -C\mathbf{I} & -\mathbf{I} \\ \mathbf{I} & \mathbf{0} \end{bmatrix}^\top dt + [\sqrt{2C} d\mathbf{w}^\top(t) \quad \mathbf{0}^\top]. \quad (27)$$

Consequently,

$$\begin{aligned} d\nabla_{\mathbf{z}(0)} \mathbf{z}^\top(t) &= \nabla_{\mathbf{z}(0)} d\mathbf{z}^\top(t) = \nabla_{\mathbf{z}(0)} \nabla^\top H(\mathbf{z}(t)) \begin{bmatrix} -C\mathbf{I} & -\mathbf{I} \\ \mathbf{I} & \mathbf{0} \end{bmatrix}^\top dt + \nabla_{\mathbf{z}(0)} [\sqrt{2C} d\mathbf{w}^\top(t) \quad \mathbf{0}^\top] \\ &= \nabla_{\mathbf{z}(0)} \nabla^\top H(\mathbf{z}(t)) \begin{bmatrix} -C\mathbf{I} & -\mathbf{I} \\ \mathbf{I} & \mathbf{0} \end{bmatrix}^\top dt = \nabla_{\mathbf{z}(0)} \mathbf{z}^\top(t) \Delta H(\mathbf{z}(t)) \begin{bmatrix} -C\mathbf{I} & -\mathbf{I} \\ \mathbf{I} & \mathbf{0} \end{bmatrix}^\top dt, \end{aligned}$$

where we use the shorthand $\Delta = \nabla \nabla^\top$. The last expression can be rewritten as

$$d\boldsymbol{\Omega}^\top(t) = \boldsymbol{\Omega}^\top(t) \begin{bmatrix} \mathbf{M}^{-1} & \mathbf{0} \\ \mathbf{0} & \Delta_\theta U(\boldsymbol{\theta}(t)) \end{bmatrix} \begin{bmatrix} -C\mathbf{I} & -\mathbf{I} \\ \mathbf{I} & \mathbf{0} \end{bmatrix}^\top dt.$$

By the rule of differentiation of determinants, we can write

$$\begin{aligned} d \det(\boldsymbol{\Omega}^\top(t)) &= \text{Tr} \left(\text{adj}(\boldsymbol{\Omega}^\top(t)) d\boldsymbol{\Omega}^\top(t) \right) = \\ &= \text{Tr} \left(\text{adj}(\boldsymbol{\Omega}^\top(t)) \boldsymbol{\Omega}^\top(t) \begin{bmatrix} \mathbf{M}^{-1} & \mathbf{0} \\ \mathbf{0} & \Delta_\theta U(\boldsymbol{\theta}(t)) \end{bmatrix} \begin{bmatrix} -C\mathbf{I} & -\mathbf{I} \\ \mathbf{I} & \mathbf{0} \end{bmatrix}^\top dt \right) = \\ &= \det(\boldsymbol{\Omega}^\top(t)) \text{Tr} \left(\begin{bmatrix} \mathbf{M}^{-1} & \mathbf{0} \\ \mathbf{0} & \Delta_\theta U(\boldsymbol{\theta}(t)) \end{bmatrix} \begin{bmatrix} -C\mathbf{I} & -\mathbf{I} \\ \mathbf{I} & \mathbf{0} \end{bmatrix}^\top dt \right) = \\ &= \det(\boldsymbol{\Omega}^\top(t)) \text{Tr} \left(\begin{bmatrix} \mathbf{M}^{-1} & \mathbf{0} \\ \mathbf{0} & \Delta_\theta U(\boldsymbol{\theta}(t)) \end{bmatrix} \begin{bmatrix} -C\mathbf{I} & \mathbf{0} \\ \mathbf{0} & \mathbf{0} \end{bmatrix}^\top dt \right) = -\det(\boldsymbol{\Omega}^\top(t)) C \text{Tr}(\mathbf{M}^{-1}) dt. \end{aligned}$$

This, together with the condition $\Omega(0) = \mathbf{I}$ proves that

$$\det(\Omega^\top(t)) = \exp(-C\text{Tr}(\mathbf{M}^{-1})t)$$

□

Having acknowledged the rich geometrical structure of Hamiltonian ODEs and SDEs, we are finally ready to introduce the concept of quasi-symplectic integrators [36], as numerical schemes that aim at preserving the underlying geometry.

Definition 3. *An numerical (stochastic) integrator $\phi : \mathbf{z}_i \rightarrow \mathbf{z}_{i+1}$ with step size η is defined to be quasi-symplectic if the following two properties holds:*

1. *The determinant of the Jacobian $\Omega = (\nabla_{\mathbf{z}_{i-1}} \phi(\mathbf{z}_i)^\top)$ of the numerical integrator does not depend on $\mathbf{z}_i = (\mathbf{r}_i, \boldsymbol{\theta}_i)$*
2. *In the limit of vanishing friction, i.e. $C \rightarrow 0$, the Jacobian Ω satisfies the symplectic condition*

$$\Omega^\top \mathbf{J} \Omega = \mathbf{J}. \quad (28)$$

In Section 5 we analyze the performance of different integration schemes (both quasi-symplectic and not) and clearly show that quasi-symplectic methods outperform non quasi-symplectic ones, in accordance with the literature [36]. Among the quasi-symplectic class, we test LEAPFROG, SYMMETRIC, LIE-TROTTER (that is quasi symplectic provided that the deterministic Hamiltonian integrator is symplectic) schemes. As for non quasi-symplectic schemes, we test the EULER and RK2 ones.

B.5 Numerical integrators

In this section, we present some examples of integrators, which we explore in the experimental Section 5 in the main paper, with their corresponding order of convergence.

B.5.1 EULER

The first scheme is the classical EULER scheme

$$\begin{cases} \boldsymbol{\theta}_i = \boldsymbol{\theta}_{i-1} + \eta \mathbf{M}^{-1} \mathbf{r}_{i-1}, \\ \mathbf{r}_i = \mathbf{r}_{i-1} - \eta C \mathbf{M}^{-1} \mathbf{r}_{i-1} - \eta \nabla U(\boldsymbol{\theta}_{i-1}) + \sqrt{2C\eta} \mathbf{w}, \quad \mathbf{w} \sim \mathcal{N}(\mathbf{0}, \mathbf{I}), \end{cases} \quad (29)$$

which has weak error of order one, and ergodic error of the same order [27]. We hereafter prove that the scheme is not quasi-symplectic. To do so we derive the Jacobian matrix

$$\Omega^\top = \nabla_{\mathbf{z}_{i-1}} \mathbf{z}_i^\top = \begin{bmatrix} \nabla_{\mathbf{r}_{i-1}} \\ \nabla_{\boldsymbol{\theta}_{i-1}} \end{bmatrix} \begin{bmatrix} \mathbf{r}_i^\top & \boldsymbol{\theta}_i^\top \end{bmatrix} = \begin{bmatrix} \mathbf{I} - \eta C \mathbf{M}^{-1} & \eta \mathbf{M}^{-1} \\ -\eta \Delta U(\boldsymbol{\theta}_{i-1}) & \mathbf{I} \end{bmatrix}, \quad (30)$$

and check that as $C \rightarrow 0$, the second requirement of quasi-symplecticity is not satisfied:

$$\begin{aligned} & \begin{bmatrix} \mathbf{I} & \eta \mathbf{M}^{-1} \\ -\eta \Delta U(\boldsymbol{\theta}_{i-1}) & \mathbf{I} \end{bmatrix} \begin{bmatrix} \mathbf{0} & -\mathbf{I} \\ \mathbf{I} & \mathbf{0} \end{bmatrix} \begin{bmatrix} \mathbf{I} & -\eta \Delta U(\boldsymbol{\theta}_{i-1}) \\ \eta \mathbf{M}^{-1} & \mathbf{I} \end{bmatrix} = \\ & \begin{bmatrix} \eta \mathbf{M}^{-1} & -\mathbf{I} \\ \mathbf{I} & \eta \Delta U(\boldsymbol{\theta}_{i-1}) \end{bmatrix} \begin{bmatrix} \mathbf{I} & -\eta \Delta U(\boldsymbol{\theta}_{i-1}) \\ \eta \mathbf{M}^{-1} & \mathbf{I} \end{bmatrix} = \begin{bmatrix} \mathbf{0} & -\mathbf{I} - \eta^2 \Delta U(\boldsymbol{\theta}_{i-1}) \\ \mathbf{I} + \eta^2 \Delta U(\boldsymbol{\theta}_{i-1}) \mathbf{M}^{-1} & \mathbf{0} \end{bmatrix} \neq \mathbf{J}. \end{aligned}$$

B.5.2 LEAPFROG

The second integrator we consider is the widely used LEAPFROG scheme

$$\begin{cases} \boldsymbol{\theta}^* = \boldsymbol{\theta}_{i-1} + \frac{\eta}{2} \mathbf{M}^{-1} \mathbf{r}_{i-1} \\ \mathbf{r}_i = \mathbf{r}_{i-1} - \eta \nabla U(\boldsymbol{\theta}^*) - \eta C \mathbf{M}^{-1} \mathbf{r}_{i-1} + \sqrt{2C\eta} \mathbf{w}, \quad \mathbf{w} \sim \mathcal{N}(\mathbf{0}, \mathbf{I}) \\ \boldsymbol{\theta}_i = \boldsymbol{\theta}^* + \frac{\eta}{2} \mathbf{M}^{-1} \mathbf{r}_i \end{cases} \quad (31)$$

This scheme is quasi-symplectic as shown hereafter. We rewrite equivalently the update scheme as a unique step as

$$\begin{cases} \mathbf{r}_i = \mathbf{r}_{i-1} - \eta \nabla U(\boldsymbol{\theta}_{i-1} + \frac{\eta}{2} \mathbf{M}^{-1} \mathbf{r}_{i-1}) - \eta C \mathbf{M}^{-1} \mathbf{r}_{i-1} + \sqrt{2C\eta} \mathbf{w} \\ \boldsymbol{\theta}_i = \boldsymbol{\theta}_{i-1} + \frac{\eta}{2} \mathbf{M}^{-1} \mathbf{r}_{i-1} + \frac{\eta}{2} \mathbf{M}^{-1} (\mathbf{r}_{i-1} - \eta \nabla U(\boldsymbol{\theta}_{i-1} + \frac{\eta}{2} \mathbf{M}^{-1} \mathbf{r}_{i-1}) - \eta C \mathbf{M}^{-1} \mathbf{r}_{i-1} + \sqrt{2C\eta} \mathbf{w}) \end{cases} \quad (32)$$

Define $\mathbf{q} = \boldsymbol{\theta}_{i-1} + \frac{\eta}{2} \mathbf{M}^{-1} \mathbf{r}_{i-1}$, $q^{(k)} = \theta_{i-1}^{(k)} + \eta m_{kp} r_{i-1}^{(p)}$, with $\mathbf{M}^{-1}|_{kp} = m_{kp}$.

$$\frac{\partial}{\partial r_{i-1}^{(m)}} \partial_n U(\mathbf{q}) = \partial_{nk} U(\mathbf{q}) \frac{q^{(k)}}{\partial r_{i-1}^{(m)}} = \partial_{nk} U(\mathbf{q}) \frac{\eta}{2} m_{kp} \delta_{pm} = \frac{\eta}{2} \partial_{nk} U(\mathbf{q}) m_{km}. \quad (33)$$

Consequently $\nabla_{\mathbf{r}_{i-1}} \nabla^\top U(\mathbf{q}) = \frac{\eta}{2} \mathbf{M}^{-1} \Delta U(\mathbf{q})$

$$\boldsymbol{\Omega}^\top = \begin{bmatrix} \mathbf{I} - \eta C \mathbf{M}^{-1} - \frac{\eta^2}{2} \mathbf{M}^{-1} \Delta U(\mathbf{q}) & \eta \mathbf{M}^{-1} - \frac{\eta^3}{4} \mathbf{M}^{-2} \Delta U(\mathbf{q}) - \frac{\eta^2}{2} C \mathbf{M}^{-2} \\ -\eta \Delta U(\mathbf{q}) & \mathbf{I} - \frac{\eta^2}{2} \mathbf{M}^{-1} \Delta U(\mathbf{q}) \end{bmatrix} \quad (34)$$

Simple algebraic manipulations show that the transposed Jacobian can be rewritten as

$$\boldsymbol{\Omega}^\top = \begin{bmatrix} \mathbf{I} & \frac{\eta}{2} \mathbf{M}^{-1} \\ \mathbf{0} & \mathbf{I} \end{bmatrix} \begin{bmatrix} \mathbf{I} - \eta C \mathbf{M}^{-1} & \mathbf{0} \\ -\eta \Delta U(\mathbf{q}) & \mathbf{I} \end{bmatrix} \begin{bmatrix} \mathbf{I} & \frac{\eta}{2} \mathbf{M}^{-1} \\ \mathbf{0} & \mathbf{I} \end{bmatrix} \quad (35)$$

The determinant of the Jacobian is then easily calculated as the product of the three determinants

$$\det(\boldsymbol{\Omega}^\top) = \det \begin{bmatrix} \mathbf{I} & \frac{\eta}{2} \mathbf{M}^{-1} \\ \mathbf{0} & \mathbf{I} \end{bmatrix} \det \begin{bmatrix} \mathbf{I} - \eta C \mathbf{M}^{-1} & \mathbf{0} \\ -\eta \Delta U(\mathbf{q}) & \mathbf{I} \end{bmatrix} \det \begin{bmatrix} \mathbf{I} & \frac{\eta}{2} \mathbf{M}^{-1} \\ \mathbf{0} & \mathbf{I} \end{bmatrix} = \det(\mathbf{I} - \eta C \mathbf{M}^{-1}), \quad (36)$$

and is independent on \mathbf{z}_0 , satisfying the first condition. By taking the limit $C \rightarrow 0$, to prove that the integrator converge to a symplectic one is sufficient to prove that

$$\begin{bmatrix} \mathbf{I} & \frac{\eta}{2} \mathbf{M}^{-1} \\ \mathbf{0} & \mathbf{I} \end{bmatrix} \begin{bmatrix} \mathbf{0} & -\mathbf{I} \\ \mathbf{I} & \mathbf{0} \end{bmatrix} \begin{bmatrix} \mathbf{I} & \frac{\eta}{2} \mathbf{M}^{-1} \\ \mathbf{0} & \mathbf{I} \end{bmatrix}^\top = \begin{bmatrix} \mathbf{0} & -\mathbf{I} \\ \mathbf{I} & \mathbf{0} \end{bmatrix}, \quad (37)$$

and that

$$\begin{bmatrix} \mathbf{I} & \mathbf{0} \\ -\eta \Delta U(\mathbf{q}) & \mathbf{I} \end{bmatrix} \begin{bmatrix} \mathbf{0} & -\mathbf{I} \\ \mathbf{I} & \mathbf{0} \end{bmatrix} \begin{bmatrix} \mathbf{I} & \mathbf{0} \\ -\eta \Delta U(\mathbf{q}) & \mathbf{I} \end{bmatrix}^\top = \begin{bmatrix} \mathbf{0} & -\mathbf{I} \\ \mathbf{I} & \mathbf{0} \end{bmatrix}. \quad (38)$$

Simple calculations show that

$$\begin{bmatrix} \mathbf{I} & \frac{\eta}{2} \mathbf{M}^{-1} \\ \mathbf{0} & \mathbf{I} \end{bmatrix} \begin{bmatrix} \mathbf{0} & -\mathbf{I} \\ \mathbf{I} & \mathbf{0} \end{bmatrix} \begin{bmatrix} \mathbf{I} & \frac{\eta}{2} \mathbf{M}^{-1} \\ \mathbf{0} & \mathbf{I} \end{bmatrix}^\top = \begin{bmatrix} \frac{\eta}{2} \mathbf{M}^{-1} & -\mathbf{I} \\ \mathbf{I} & \mathbf{0} \end{bmatrix} \begin{bmatrix} \mathbf{I} & \mathbf{0} \\ \frac{\eta}{2} \mathbf{M}^{-1} & \mathbf{I} \end{bmatrix} = \begin{bmatrix} \mathbf{0} & -\mathbf{I} \\ \mathbf{I} & \mathbf{0} \end{bmatrix},$$

and similarly we can prove eq. Eq. (38), completing the proof that LEAPFROG is quasi-symplectic. This integrator has a theoretical order of convergence equal to one but its performance are on par with other order two integrators. See also E.2 for a detailed discussion.

B.5.3 RK2

We then consider the Runge-Kutta scheme of second order [27]

$$\begin{cases} \boldsymbol{\theta}^* = \boldsymbol{\theta}_{i-1} + \eta \mathbf{M}^{-1} \mathbf{r}_{i-1} \\ \mathbf{r}^* = \mathbf{r}_{i-1} - \eta \nabla U(\boldsymbol{\theta}_{i-1}) - \eta C \mathbf{M}^{-1} \mathbf{r}_{i-1} + \sqrt{2C\eta} \mathbf{w}, \quad \mathbf{w} \sim \mathcal{N}(\mathbf{0}, \mathbf{I}) \\ \boldsymbol{\theta}_i = \boldsymbol{\theta}_{i-1} + \frac{\eta}{2} (\mathbf{M}^{-1} \mathbf{r}_{i-1} + \mathbf{M}^{-1} \mathbf{r}^*) \\ \mathbf{r}_i = \mathbf{r}_{i-1} + \frac{\eta}{2} (-\nabla U(\boldsymbol{\theta}_{i-1}) - C \mathbf{r}_{i-1} - \nabla U(\boldsymbol{\theta}^*) - C \mathbf{r}^*) + \sqrt{2C\eta} \mathbf{w} \end{cases} \quad (39)$$

The order of convergence can be derived as in [27],[36]. The scheme is not quasi-symplectic, as discussed also in [36].

B.5.4 LIE-TROTTER

Finally we consider an order-two Lie-Trotter splitting scheme [2]

$$\begin{cases} \boldsymbol{\theta}^* = \boldsymbol{\theta}_{i-1} + \frac{\eta}{2} \mathbf{M}^{-1} \mathbf{r}_{i-1} \\ \mathbf{r}^* = \mathbf{r}_{i-1} - \eta \nabla U(\boldsymbol{\theta}^*) \\ \boldsymbol{\theta}^i = \boldsymbol{\theta}^* + \frac{\eta}{2} \mathbf{M}^{-1} \mathbf{r}^* \\ \mathbf{r}_i = \exp(-C \mathbf{M}^{-1} \eta) \mathbf{r}^* + \sqrt{\mathbf{M}(1 - \exp(-2C \mathbf{M}^{-1} \eta))} \mathbf{w}, \quad \mathbf{w} \sim \mathcal{N}(\mathbf{0}, \mathbf{I}) \end{cases} \quad (40)$$

We choose the particular case of a deterministic leapfrog for the Hamiltonian integration, but any other integrator ψ would have been valid. To derive the order of convergence it is sufficient to use the result of Theorem 4 as in [1].

The scheme can be interpreted as the cascade of a purely deterministic symplectic integrator (the leapfrog step)

$$\begin{cases} \mathbf{r}_{i-1} \\ \boldsymbol{\theta}_{i-1} \end{cases} \rightarrow \begin{cases} \mathbf{r}^* = \mathbf{r}_{i-1} - \eta \nabla U(\boldsymbol{\theta}_{i-1} + \frac{\eta}{2} \mathbf{M}^{-1} \mathbf{r}_{i-1}) \\ \boldsymbol{\theta}^* = \boldsymbol{\theta}_{i-1} + \frac{\eta}{2} \mathbf{M}^{-1} \mathbf{r}_{i-1} + \frac{\eta}{2} \mathbf{M}^{-1} (\mathbf{r}_{i-1} - \eta \nabla U(\boldsymbol{\theta}_{i-1} + \frac{\eta}{2} \mathbf{M}^{-1} \mathbf{r}_{i-1})) \end{cases} \quad (41)$$

and the analytic step

$$\begin{cases} \mathbf{r}^* \\ \boldsymbol{\theta}^* \end{cases} \rightarrow \begin{cases} \mathbf{r}_i = \exp(-C \mathbf{M}^{-1} \eta) \mathbf{r}^* + \sqrt{\mathbf{M}(1 - \exp(-2C \mathbf{M}^{-1} \eta))} \mathbf{w} \\ \boldsymbol{\theta}_i = \boldsymbol{\theta}^* \end{cases} \quad (42)$$

With calculations similar to the ones in Section B.5.2 it is easy to show that the purely deterministic leapfrog step is symplectic, i.e., its Jacobian $\boldsymbol{\Omega}_1$ satisfies $\boldsymbol{\Omega}_1^\top \mathbf{J} \boldsymbol{\Omega}_1 = \mathbf{J}$.

Concerning the analytical step instead, it is easy to show that the Jacobian of the transformation is equal to

$$\boldsymbol{\Omega}_2^\top = \begin{bmatrix} \exp(-C \mathbf{M}^{-1} \eta) & \mathbf{0} \\ \mathbf{0} & \mathbf{I} \end{bmatrix}. \quad (43)$$

Consequently, the overall Jacobian of the two steps taken jointly is

$$\boldsymbol{\Omega}^\top = \boldsymbol{\Omega}_1^\top \boldsymbol{\Omega}_2^\top \quad (44)$$

and it is easily shown to be satisfying the two requirements for the quasi-symplecticity. The LIE-TROTTER scheme is then quasi-symplectic.

C Additional derivations for Section 3

We present the Baker–Campbell–Hausdorff in Appendix C.1, useful for technical derivations in the rest of the section. Appendix C.2 contains results on the average of back and forth of multiple operators (Theorem 6). In Appendix C.3 we study the effect of chaining multiple (different) numerical integrators. Finally, Appendix C.4 combines the elements of the previous Sections to provide the proof for Theorem 2. Appendix C.5 contains the Proof of Theorem 3.

C.1 Baker–Campbell–Hausdorff formula

We here present the Baker–Campbell–Hausdorff formula, and in particular the series expansion due to [15], that will prove useful in the technical derivations. Given two differential operators \mathcal{A}, \mathcal{B} , we have that

$$\exp(\mathcal{A}) \exp(\mathcal{B}) = \exp(\mathcal{Z}) \quad (45)$$

where $\mathcal{Z} = \mathcal{A} + \mathcal{B} + \frac{1}{2}[\mathcal{A}, \mathcal{B}] + \frac{1}{12}([\mathcal{A}, [\mathcal{A}, \mathcal{B}]] + [\mathcal{B}, [\mathcal{B}, \mathcal{A}]] - \frac{1}{24}[\mathcal{B}, [\mathcal{A}, [\mathcal{A}, \mathcal{B}]]) - \frac{1}{720}([\mathcal{B}, [\mathcal{B}, [\mathcal{B}, [\mathcal{B}, \mathcal{A}]]]] + [\mathcal{A}, [\mathcal{A}, [\mathcal{A}, [\mathcal{A}, \mathcal{B}]]]]) + \frac{1}{360}([\mathcal{A}, [\mathcal{B}, [\mathcal{B}, [\mathcal{B}, \mathcal{A}]]]] + [\mathcal{B}, [\mathcal{A}, [\mathcal{A}, [\mathcal{A}, \mathcal{B}]]]]) + \frac{1}{120}([\mathcal{B}, [\mathcal{A}, [\mathcal{B}, [\mathcal{A}, \mathcal{B}]]]] + [\mathcal{A}, [\mathcal{B}, [\mathcal{A}, [\mathcal{B}, \mathcal{A}]]]]) + \dots$

C.2 Average of back and forth operators

The following Theorem provides a technical support for the proofs of the order of convergence of chains of operators.

Theorem 6. *Suppose the differential operator \mathcal{L} admits the following decomposition:*

$$\mathcal{L} = \sum_{i=1}^K \mathcal{L}_i, \quad (46)$$

Then the equivalent operator \mathcal{P} obtained by averaging the back $\left(\text{i.e. } \prod_{i=1}^K \exp(\eta \mathcal{L}_i) \right)$ and the forth $\left(\text{i.e. } \prod_{i=K}^1 \exp(\eta \mathcal{L}_i) \right)$ evolution of the single terms has local error $\mathcal{O}(\eta^3)$ for the operator $\exp(\eta \mathcal{L})$, i.e.

$$\mathcal{P} = \frac{\prod_{i=K}^1 \exp(\eta \mathcal{L}_i) + \prod_{i=1}^K \exp(\eta \mathcal{L}_i)}{2} = \exp(\eta \mathcal{L}) + \mathcal{O}(K\eta^3). \quad (47)$$

Proof. The proof of Theorem 6 is as follows:

$$\exp(\eta \mathcal{L}_i) = \mathcal{I} + \eta \mathcal{L}_i + \frac{\eta^2 \mathcal{L}_i^2}{2} + \mathcal{O}(\eta^3) \quad (48)$$

Consequently:

$$\prod_{i=1}^K \left(\mathcal{I} + \eta \mathcal{L}_i + \frac{\eta^2 \mathcal{L}_i^2}{2} + \mathcal{O}(\eta^3) \right) = \mathcal{I} + \eta \sum_{i=1}^K \mathcal{L}_i + \frac{\eta^2}{2} \sum_{i=1}^K \mathcal{L}_i^2 + \eta^2 \sum_{\substack{i_1=1 \dots K-1, \\ i_2=i_1+1 \dots K}} \mathcal{L}_{i_1} \mathcal{L}_{i_2} + \mathcal{O}((K-1)\eta^3) \quad (49)$$

and

$$\prod_{i=K}^1 \left(\mathcal{I} + \eta \mathcal{L}_i + \frac{\eta^2 \mathcal{L}_i^2}{2} + \mathcal{O}(\eta^3) \right) = \mathcal{I} + \eta \sum_{i=1}^K \mathcal{L}_i + \frac{\eta^2}{2} \sum_{i=1}^K \mathcal{L}_i^2 + \eta^2 \sum_{\substack{i_1=2 \dots K, \\ i_2=1 \dots i_1-1}} \mathcal{L}_{i_1} \mathcal{L}_{i_2} + \mathcal{O}((K-1)\eta^3) \quad (50)$$

The fundamental equality of interest is:

$$\begin{aligned} \mathcal{L}^2 &= \left(\sum_{i_1=1}^K \mathcal{L}_{i_1} \right) \left(\sum_{i_2=1}^K \mathcal{L}_{i_2} \right) = \left(\sum_{\substack{i_1=1 \dots K, \\ i_2=1 \dots K}} \mathcal{L}_{i_1} \mathcal{L}_{i_2} \right) = \left(\sum_{\substack{i_1=1 \dots K, \\ i_2=i_1 \dots K}} \mathcal{L}_{i_1} \mathcal{L}_{i_2} + \sum_{\substack{i_1=1 \dots K, \\ i_2=1 \dots i_1-1}} \mathcal{L}_{i_1} \mathcal{L}_{i_2} \right) \\ &= \left(\sum_{\substack{i_1=1 \dots K, \\ i_2=i_1}} \mathcal{L}_{i_1} \mathcal{L}_{i_2} + \sum_{\substack{i_1=1 \dots K, \\ i_2=i_1+1 \dots K}} \mathcal{L}_{i_1} \mathcal{L}_{i_2} + \sum_{\substack{i_1=1 \dots K, \\ i_2=1 \dots i_1-1}} \mathcal{L}_{i_1} \mathcal{L}_{i_2} \right) \\ &= \left(\sum_{\substack{i_1=1 \dots K, \\ i_2=i_1}} \mathcal{L}_{i_1} \mathcal{L}_{i_2} + \sum_{\substack{i_1=1 \dots K, \\ i_2=i_1+1 \dots K}} \mathcal{L}_{i_1} \mathcal{L}_{i_2} + \sum_{\substack{i_1=2 \dots K, \\ i_2=1 \dots i_1-1}} \mathcal{L}_{i_1} \mathcal{L}_{i_2} \right) \end{aligned}$$

By means of simple algebraic considerations we can thus obtain the desired result, as

$$\begin{aligned}
\mathcal{P} &= \frac{\prod_{i=K}^1 \exp(\eta \mathcal{L}_i) + \prod_{i=1}^K \exp(\eta \mathcal{L}_i)}{2} \\
&= \frac{\prod_{i=1}^K \left(\mathcal{I} + \eta \mathcal{L}_i + \frac{\eta^2 \mathcal{L}_i^2}{2} + \mathcal{O}(\eta^3) \right) + \prod_{i=K}^1 \left(\mathcal{I} + \eta \mathcal{L}_i + \frac{\eta^2 \mathcal{L}_i^2}{2} + \mathcal{O}(\eta^3) \right)}{2} \\
&= \mathcal{I} + \eta \sum_{i=1}^K \mathcal{L}_i + \frac{\eta^2}{2} \left(\left(\sum_{i_1=1}^K \mathcal{L}_{i_1} \right) \left(\sum_{i_2=1}^K \mathcal{L}_{i_2} \right) \right) + \mathcal{O}((K-1)\eta^3) = \exp(\eta \mathcal{L}) + \mathcal{O}(K\eta^3)
\end{aligned}$$

□

C.3 Randomized sequence of numerical integration steps

The first aspect we consider is the net effect of chaining multiple (different) numerical integrators on the transformation of ϕ .

Theorem 7. Consider a set of numerical integrators $\{\psi_i\}_{i=1}^K$ with corresponding functionals \mathcal{U}_i . If we build the stochastic variable \mathbf{z}_{fin} starting from \mathbf{z}_0 through the following chain

$$\mathbf{z}_{fin} = \psi_K(\psi_{K-1}(\dots \psi_1(\mathbf{z}_0))), \quad (51)$$

then the generic function ϕ is transformed as follows

$$\mathbb{E}[\phi(\mathbf{z}_{fin})] = \mathcal{U}_1 \mathcal{U}_2 \dots \mathcal{U}_K \phi(\mathbf{z}_0) \quad (52)$$

Notice the backward order of the differential operators and the difference with the ordering assumed in [9].

Proof. We give the proof for $K = 2$ since the general result is trivially extended from this case. In this case $\mathbf{z}_{fin} = \psi_2(\psi_1(\mathbf{z}_0))$. Define $\mathbf{z}_1 = \psi_1(\mathbf{z}_0)$. Since

$$\begin{aligned}
\mathbb{E}[\phi(\mathbf{z}_{fin})] &= \int \phi(\mathbf{z}_{fin}) p(\mathbf{z}_{fin} | \mathbf{z}_0) d\mathbf{z}_{fin} = \int \phi(\mathbf{z}_{fin}) p(\mathbf{z}_{fin} | \mathbf{z}_1) p(\mathbf{z}_1 | \mathbf{z}_0) d\mathbf{z}_1 d\mathbf{z}_{fin} = \\
&= \int \left(\int \phi(\mathbf{z}_{fin}) p(\mathbf{z}_{fin} | \mathbf{z}_1) d\mathbf{z}_{fin} \right) p(\mathbf{z}_1 | \mathbf{z}_0) d\mathbf{z}_1 = \int (\mathcal{U}_2 \phi(\mathbf{z}_1)) p(\mathbf{z}_1 | \mathbf{z}_0) d\mathbf{z}_1 = \mathcal{U}_1 \mathcal{U}_2 \phi(\mathbf{z}_0)
\end{aligned}$$

the result is proven. □

Next, we consider the case in which we consider different chains of numerical integrators and apply one of them according to some probability distribution.

Theorem 8. Consider multiple sets of numerical integrators $\{\psi_{i,j}\}_{i=1}^K$ with corresponding functionals $\mathcal{U}_{i,j}$, with $j = 1 \dots S$. Choose an index $j^* \in [1, \dots, S]$ according to some probability distribution $p(j^* = j) = w_j$. Build the stochastic variable \mathbf{z}_{fin} starting from \mathbf{z}_0 through the chain corresponding to the sampled index

$$\mathbf{z}_{fin} = \psi_{K,j^*}(\psi_{K-1,j^*}(\dots \psi_{1,j^*}(\mathbf{z}_0))), \quad (53)$$

then the generic function ϕ is transformed as follows

$$\mathbb{E}[\phi(\mathbf{z}_{fin})] = \sum_{j=1}^S w_j \mathcal{U}_{1,j} \mathcal{U}_{2,j} \dots \mathcal{U}_{K,j} \phi(\mathbf{z}_0). \quad (54)$$

The result is trivially derived considering the previous theorem and the law of total expectation. Indeed

$$\begin{aligned}
\mathbb{E}[\phi(\mathbf{z}_{fin})] &= \mathbb{E}_{j^*} [\mathbb{E}[\phi(\psi_{K,j^*}(\psi_{K-1,j^*}(\dots \psi_{1,j^*}(\mathbf{z}_0)))))] = \\
&= \mathbb{E}_{j^*} [\mathcal{U}_{1,j^*} \mathcal{U}_{2,j^*} \dots \mathcal{U}_{K,j^*} \phi(\mathbf{z}_0)] = \sum_{j=1}^S w_j \mathcal{U}_{1,j} \mathcal{U}_{2,j} \dots \mathcal{U}_{K,j} \phi(\mathbf{z}_0).
\end{aligned}$$

C.4 Proof of Theorem 2

As stated in Theorem 2, we consider numerical integrators ψ_i with order p . Consequently, we have representation $\mathcal{U}_i = \exp(\eta\mathcal{L}_i) + \mathcal{O}(\eta^{p+1})$ of the operators \mathcal{U}_i corresponding to the integrators ψ_i . The proof of Theorem 2 is obtained considering Theorem 6 and Theorem 8.

Consider $K!$ sets of numerical integrators as follows:

$$\{\psi_{\pi_1^1}\}_{i=1}^K, \quad \{\psi_{\pi_2^2}\}_{i=1}^K, \dots, \{\psi_{\pi_{K!}^{K!}}\}_{i=1}^K, \quad (55)$$

where $\pi^1, \dots, \pi^{K!}$ are all the possible permutations of the K operators, sampled uniformly with probability $\frac{1}{K!}$. If, in accordance with the hypotheses of Theorem 2, the initial condition has stochastic evolution through a chain of randomly permuted integrators, then the propagation operator is:

$$\mathcal{U} = \sum_{i=1}^{K!} \frac{1}{K!} \mathcal{U}_{\pi_K^i} \mathcal{U}_{\pi_{K-1}^i} \dots \mathcal{U}_{\pi_1^i}. \quad (56)$$

The proof is a direct consequence of Theorem 8.

It is obviously possible to rewrite the set of all possible permutations as the union of two sets of equal cardinality, such that each element of one of the two set has a (unique) element of the other set that is its lexicographic reverse.

$$\begin{aligned} &\{\psi_{\pi_1^1}\}_{i=1}^K, \quad \{\psi_{\pi_2^2}\}_{i=1}^K, \dots, \{\psi_{\pi_{K!/2}^{K!/2}}\}_{i=1}^K \\ &\{\psi_{\pi_1^1}\}_{i=K}^1, \quad \{\psi_{\pi_2^2}\}_{i=K}^1, \dots, \{\psi_{\pi_{K!/2}^{K!/2}}\}_{i=K}^1. \end{aligned}$$

We rewrite the sum then as:

$$\mathcal{U} = \sum_{i=1}^{K!/2} \frac{2}{K!} \left(\frac{1}{2} \mathcal{U}_{\pi_K^i} \mathcal{U}_{\pi_{K-1}^i} \dots \mathcal{U}_{\pi_1^i} + \frac{1}{2} \mathcal{U}_{\pi_1^i} \mathcal{U}_{\pi_2^i} \dots \mathcal{U}_{\pi_K^i} \right).$$

Then, by Theorem 6, since:

$$\frac{1}{2} \mathcal{U}_{\pi_K^i} \mathcal{U}_{\pi_{K-1}^i} \dots \mathcal{U}_{\pi_1^i} + \frac{1}{2} \mathcal{U}_{\pi_1^i} \mathcal{U}_{\pi_2^i} \dots \mathcal{U}_{\pi_K^i} = \exp(\eta\mathcal{L}) + \mathcal{O}(K\eta^{\min(p+1,3)}), \quad (57)$$

we have

$$\mathcal{U} = \exp(\eta\mathcal{L}) + \mathcal{O}(K\eta^{\min(p+1,3)}). \quad (58)$$

C.5 Proof of Theorem 3

We are considering numerical integrators whose corresponding operators are

$$\mathcal{U}_i = \exp(\eta\mathcal{L}_i) + \mathcal{O}(\eta^{p+1}) \quad (59)$$

Applying the randomized ordering scheme to the considered setting induces then an operator (Theorem 2)

$$\mathcal{U} = \exp(\eta\mathcal{L}) + \mathcal{O}(K\eta^{\min(p+1,3)}) \quad (60)$$

that we can expand as

$$\mathcal{U} = \mathcal{I} + \eta\mathcal{L} + \frac{\eta^2}{2}\mathcal{L}^2 + \mathcal{O}(K\eta^{\min(p+1,3)}) \quad (61)$$

Then, the application of Theorem 4 provides the desired result.

D Additional derivations for Section 4

D.1 Proof of HMC convergence rate

We shall rewrite for simplicity the HMC scheme

$$\mathbf{z}^* = \left[\mathbf{r}^{*\top}, \boldsymbol{\theta}^{*\top} \right]^\top = \underbrace{\psi(\dots \psi(\psi(\mathbf{z}_0)))}_{N_t \text{ times}}, \quad \left[\mathbf{r}_1^\top, \boldsymbol{\theta}_1^\top \right] = \left[\alpha \mathbf{r}^{*\top} + \sqrt{1 - \alpha^2} \mathbf{w}^\top, \boldsymbol{\theta}^{*\top} \right]. \quad (62)$$

The proof of the equivalence between HMC and a variant of LIE-TROTTER scheme, including its convergence rate, is trivial by construction.

The classical LIE-TROTTER scheme consists in alternating steps of pure \mathcal{H} dynamics, considering a numerical integrator ψ , and \mathcal{D} dynamics, that can be solved exactly, as follows

$$\mathbf{z}^* = [\mathbf{r}^{*\top}, \boldsymbol{\theta}^{*\top}]^\top = \psi(\mathbf{z}_0), \quad [\mathbf{r}_1^\top, \boldsymbol{\theta}_1^\top] = [\exp(-C\eta)\mathbf{r}^* + \sqrt{1 - \exp(-2C\eta)}\mathbf{w}, \boldsymbol{\theta}^{*\top}]. \quad (63)$$

Similarly, it is possible to construct a LIE-TROTTER scheme in which N_l steps of \mathcal{H} dynamics and N_l steps of \mathcal{D} dynamics are alternated, providing the following scheme

$$\mathbf{z}^* = [\mathbf{r}^{*\top}, \boldsymbol{\theta}^{*\top}]^\top = \underbrace{\psi(\dots \psi(\psi(\mathbf{z}_0)))}_{N_l \text{ times}},$$

$$[\mathbf{r}_1^\top, \boldsymbol{\theta}_1^\top] = [\exp(-CN_l\eta)\mathbf{r}^{*\top} + \sqrt{1 - \exp(-2CN_l\eta)}\mathbf{w}^\top, \boldsymbol{\theta}^{*\top}]. \quad (64)$$

It is then evident that (64) and (62) correspond to the same scheme when considering $\alpha = \exp(-CN_l\eta)$.

Having shown the equivalence between the two schemes, we can proceed providing the convergence rates with the machinery considered in this work. We consider the scheme (64). The pure Hamiltonian steps transform the functions ϕ with operator

$$\mathcal{P} = \exp(\eta N_l \mathcal{H}) + \mathcal{O}(N_l \eta^{p+1}). \quad (65)$$

The dynamics of an SDE with generator term \mathcal{D} are simulated exactly, and consequently the overall operator that transforms the ϕ functions can then be expressed as

$$\mathcal{U} = \mathcal{P} \exp(\eta N_l \mathcal{D}) = (\exp(\eta N_l \mathcal{H}) + \mathcal{O}(N_l \eta^{p+1})) \exp(\eta N_l \mathcal{D}) = \exp(\eta N_l \mathcal{H}) \exp(\eta N_l \mathcal{D}) + \mathcal{O}(N_l \eta^{p+1}).$$

We expand in Taylor series (look at [2] for a similar exposition) the terms of the product

$$\exp(\eta N_l \mathcal{H}) \exp(\eta N_l \mathcal{D}) = \sum_{n=0}^{\infty} \eta^n \frac{(N_l \mathcal{H})^n}{n!} \sum_{m=0}^{\infty} \eta^m \frac{(N_l \mathcal{D})^m}{m!} = \sum_{k=0}^{\infty} \eta^k \left(\sum_{n+m=k} \frac{(N_l \mathcal{H})^n}{n!} \frac{(N_l \mathcal{D})^m}{m!} \right).$$

Simple operator algebra shows that

$$(\exp(\eta N_l \mathcal{H}) \exp(\eta N_l \mathcal{D}))^\dagger = \sum_{k=0}^{\infty} \eta^k \left(\sum_{n+m=k} \frac{(N_l \mathcal{D}^\dagger)^m}{m!} \frac{(N_l \mathcal{H}^\dagger)^n}{n!} \right). \quad (66)$$

Then we truncate represent the operator \mathcal{U} up to order $\mathcal{O}(\eta^{p+1})$ as

$$\mathcal{U} = \sum_{k=0}^p \eta^k \left(\sum_{n+m=k} \frac{(N_l \mathcal{D}^\dagger)^m}{m!} \frac{(N_l \mathcal{H}^\dagger)^n}{n!} \right) + \mathcal{O}(N_l \eta^{p+1}). \quad (67)$$

We use the fact that $\mathcal{H}^\dagger \rho_{ss} = \mathcal{D}^\dagger \rho_{ss} = 0$ and with the help of Theorem 4 prove the desired result.

As mentioned in the main paper, the most commonly used implementation of HMC is the classical one, in which full momentum resampling is considered, i.e. $\alpha = 0$. Considering that it is possible to obtain $\alpha = 0$ in the regime $C \rightarrow \infty$, we can immediately understand how, from a schematical point of view, HMC with full momentum resampling can be interpreted as a variation of the LIE-TROTTER scheme.

Although a naive interpretation of the equivalent operator induced by the HMC scheme with full momentum resampling would suggests that the order of convergence is the same $\left(\lim_{C \rightarrow \infty} \mathcal{U} \right)^\dagger \rho_{ss} = \left(\lim_{C \rightarrow \infty} \mathcal{U}^\dagger \rho_{ss} \right)$, the precise derivation would require a careful analysis of the joint limit $C \rightarrow \infty, \eta \rightarrow 0$ with the constraint $\eta C \rightarrow \infty$. The precise exploration of this regime is outside the scope of the paper, and we simply conjecture that the performance of HMC with full momentum resampling will be at best as good as the performance with partial momentum resampling, for which the convergence rate is provided.

E A detailed look into LEAPFROG

E.1 Analytical solution of Ornstein-Uhlenbeck process

We here derive the analytical solution of an Ornstein-Uhlenbeck process for the analytical steps of certain numerical schemes. The process under study has the following form

$$d\mathbf{r}(t) = -C\mathbf{M}^{-1}\mathbf{r}(t)dt - \mathbf{f}dt + \sqrt{2C}\mathbf{dw}(t) \quad (68)$$

that can be rewritten, with $\boldsymbol{\mu} = (C\mathbf{M}^{-1})^{-1}\mathbf{f}$, as

$$d\mathbf{r}(t) = -C\mathbf{M}^{-1}(\mathbf{r}(t) - \boldsymbol{\mu})dt + \sqrt{2C}\mathbf{dw}(t) \quad (69)$$

that has analytic solution

$$\mathbf{r}(t) = \exp(-C\mathbf{M}^{-1}t)(\mathbf{r}(0) - \boldsymbol{\mu}) + \boldsymbol{\mu} + \sqrt{2C} \int_0^t \exp(-C\mathbf{M}^{-1}(t-s))\mathbf{dw}(s) \quad (70)$$

By taking the differential of Eq. (70) indeed

$$\begin{aligned} d\mathbf{r}(t) &= -C\mathbf{M}^{-1} \exp(-C\mathbf{M}^{-1}t)(\mathbf{r}(0) - \boldsymbol{\mu}) + \sqrt{2C} \exp(-C\mathbf{M}^{-1}(t-t))\mathbf{dw}(t) \\ &\quad - C\mathbf{M}^{-1}\sqrt{2C} \int_0^t \exp(-C\mathbf{M}^{-1}(t-s))\mathbf{dw}(s) \\ &= -C\mathbf{M}^{-1} \left(\exp(-C\mathbf{M}^{-1}t)(\mathbf{r}(0) - \boldsymbol{\mu}) + \sqrt{2C} \int_0^t \exp(-C\mathbf{M}^{-1}(t-s))\mathbf{dw}(s) \right) + \sqrt{2C}\mathbf{dw}(t) = \\ &\quad - C\mathbf{M}^{-1}(\mathbf{r}(t) - \boldsymbol{\mu})dt + \sqrt{2C}\mathbf{dw}(t). \end{aligned}$$

The $\boldsymbol{\mu}$ term in the solution is added to ensure the consistency with initial conditions,

$$\mathbf{r}(0) = (\mathbf{r}(0) - \boldsymbol{\mu}) + \boldsymbol{\mu} + \mathbf{0} = \mathbf{r}(0) \quad (71)$$

To derive the “algorithmic” version it is necessary to compute the variance of the noise term at a given time instant

$$\begin{aligned} &\sqrt{2C} \int_0^t \exp(-C\mathbf{M}^{-1}(t-s))\mathbf{dw}(s) \sqrt{2C} \int_0^t \exp(-C\mathbf{M}^{-1}(t-q))\mathbf{dw}(q) = \\ &2C \int_0^t \exp(-2C\mathbf{M}^{-1}(t-s))ds = 2C \exp(-2C\mathbf{M}^{-1}t) \int_0^t \exp(2C\mathbf{M}^{-1}s)ds = \\ &2C \exp(-2C\mathbf{M}^{-1}t) (\exp(2C\mathbf{M}^{-1}t) - \mathbf{I}) (2C\mathbf{M}^{-1})^{-1} = \mathbf{M}(\mathbf{I} - \exp(-2C\mathbf{M}^{-1}t)), \end{aligned}$$

providing an equivalent representation

$$\mathbf{r}(t) = \exp(-C\mathbf{M}^{-1}t)(\mathbf{r}(0) - \boldsymbol{\mu}) + \boldsymbol{\mu} + \sqrt{\mathbf{M}(1 - \exp(-2C\mathbf{M}^{-1}t))}\mathbf{w}, \quad \mathbf{w} \sim \mathcal{N}(\mathbf{0}, \mathbf{I}). \quad (72)$$

When \mathbf{M} is diagonal, the exponential matrix is diagonal with entries obtained by exponentiating its diagonal elements.

The Stochastic Position verlet scheme (order-two, the "correct" leapfrog) can then be derived as

$$\begin{cases} \boldsymbol{\theta}^* = \boldsymbol{\theta}_0 + \frac{\eta}{2}\mathbf{M}^{-1}\mathbf{r}_0 \\ \mathbf{r}_1 = \exp(-C\mathbf{M}^{-1}\eta)\mathbf{r}_0 + (\mathbf{I} - \exp(-C\mathbf{M}^{-1}\eta)) \frac{\mathbf{M}}{C} \nabla U(\boldsymbol{\theta}^*) + \sqrt{\mathbf{M}(1 - \exp(-2C\mathbf{M}^{-1}\eta))}\mathbf{w} \\ \boldsymbol{\theta}_1 = \boldsymbol{\theta}^* + \frac{\eta}{2}\mathbf{M}^{-1}\mathbf{r}_1. \end{cases} \quad (73)$$

E.2 Detailed LEAPFROG analysis

The purpose of this section is to explore in detail the mathematical properties of the LEAPFROG scheme, the most commonly adopted numerical integrator in the Bayesian sampling community.

The deterministic LEAPFROG is a known deterministic integrator. When considering SDEs, it is possible to derive its stochastic counterpart as a blind generalization of the deterministic leapfrog scheme, i.e. starting from

$$\begin{cases} \boldsymbol{\theta}^* = \boldsymbol{\theta}_0 + \frac{\eta}{2} \mathbf{M}^{-1} \mathbf{r}_0 \\ \mathbf{r}_1 = \mathbf{r}_0 - \eta \nabla U(\boldsymbol{\theta}^*) \\ \boldsymbol{\theta}_1 = \boldsymbol{\theta}^* + \frac{\eta}{2} \mathbf{M}^{-1} \mathbf{r}_1 \end{cases} \quad (74)$$

the following scheme is constructed

$$\begin{cases} \boldsymbol{\theta}^* = \boldsymbol{\theta}_0 + \frac{\eta}{2} \mathbf{M}^{-1} \mathbf{r}_0 \\ \mathbf{r}_1 = \mathbf{r}_0 - \eta \nabla U(\boldsymbol{\theta}^*) - \eta C \mathbf{r}_0 + \sqrt{2C\eta} \mathbf{w}, \quad \mathbf{w} \sim \mathcal{N}(\mathbf{0}, \mathbf{I}) \\ \boldsymbol{\theta}_1 = \boldsymbol{\theta}^* + \frac{\eta}{2} \mathbf{M}^{-1} \mathbf{r}_1. \end{cases} \quad (75)$$

Notice that in practical implementations the first and last step are merged into a single step with the exception of the beginning and end of the chain. This does not pose a problem in that usually we are interested only in functions of the position.

Importantly, the deterministic LEAPFROG is order-two. The steps of the scheme Eq. (74) are analytic solutions of differential equations, and the integration induces operators

$$\exp\left(\frac{\eta}{2} (\nabla_{\mathbf{r}}^\top T(\mathbf{r})) \nabla_{\boldsymbol{\theta}}\right) \exp\left(-\eta (\nabla_{\boldsymbol{\theta}}^\top U(\boldsymbol{\theta})) \nabla_{\mathbf{r}}\right) \exp\left(\frac{\eta}{2} (\nabla_{\mathbf{r}}^\top T(\mathbf{r})) \nabla_{\boldsymbol{\theta}}\right) = \exp(\eta \mathcal{H}) + \mathcal{O}(\eta^3). \quad (76)$$

The result is immediate remembering that $\mathcal{H} = -(\nabla_{\boldsymbol{\theta}}^\top U(\boldsymbol{\theta})) \nabla_{\mathbf{r}} + (\nabla_{\mathbf{r}}^\top T(\mathbf{r})) \nabla_{\boldsymbol{\theta}}$ and using the BCH formula Appendix C.1.

The stochastic LEAPFROG, Eq. (75), instead, is order-one. While the position update steps are analytic, the momentum update

$$\mathbf{r}_1 = \mathbf{r}_0 - \eta \nabla U(\boldsymbol{\theta}^*) - \eta C \mathbf{r}_0 + \sqrt{2C\eta} \mathbf{w} \quad (77)$$

is not anymore an analytic step but it is an EULER step, thus with an error $\mathcal{O}(\eta^2)$. Consequently, the scheme of Eq. (75) induces an operator as follows

$$\exp\left(\frac{\eta}{2} \mathcal{D}\right) (\exp(\eta \mathcal{H}) + \mathcal{O}(\eta^2)) \exp\left(\frac{\eta}{2} \mathcal{D}\right) = \exp(\eta \mathcal{L}) + \mathcal{O}(\eta^{\min(2,3)}) = \exp(\eta \mathcal{L}) + \mathcal{O}(\eta^2). \quad (78)$$

Despite being formally order-one, we found no empirical difference between the stochastic LEAPFROG scheme and other quasi-symplectic order-two schemes. Similar results have been observed in the SDE simulation literature, look for example at [36], Table 1. The possible explanation is that while the stochastic LEAPFROG is not order-two, it is nevertheless a quasi symplectic scheme. This important geometrical property can explain the robustness of the scheme.

Here we explore the differential operator \mathcal{U} , $\mathbb{E}[\phi(\mathbf{z}_1)|\mathbf{z}_0] = \mathcal{U}\phi$ explicitly, by expanding it in Taylor series and comparing it with the expansion of the true operator $\exp(\eta \mathcal{L})$. As expected, we explicitly prove that the integrator is at least order-one.

We consider the Taylor expansion of the operator \mathcal{U} induced by the numerical scheme and focus on the η^2 terms. To be exactly of order two, we would need the combination of such terms to be equal to \mathcal{L}^2 . To check whether this holds or not, we compare the expansion of \mathcal{U} , Eq. (79), and the operator \mathcal{L}^2 , Eq. (80), and verify indeed that there is not a matching, according to the statement that LEAPFROG is order one. We believe however that the explanation of the performance of LEAPFROG scheme, on par with other second order schemes, can be understood by considering that many of the summands of Eq. (79), Eq. (80) coincide and that the scheme is quasi-symplectic. Our is however an educated guess at best, and not a mathematical proof. The interested reader could use our discussion as a starting point for a precise analysis.

For simplicity, we expose our reasoning for the one-dimensional case. We define $f = \frac{\partial U}{\partial \theta}$, and we start by manipulating the expression for the value of \mathbf{z}_1 :

$$\begin{aligned} \begin{bmatrix} r_1 \\ \theta_1 \end{bmatrix} &= \begin{bmatrix} r_0 - \eta f(\theta_0 + \frac{\eta}{2} r_0) - \eta C r_0 + \sqrt{2C\eta} w \\ \theta_0 + \frac{\eta}{2} r_0 + \frac{\eta}{2} (r_0 - \eta f(\theta_0 + \frac{\eta}{2} r_0) - \eta C r_0 + \sqrt{2C\eta} w) \end{bmatrix} = \\ &= \begin{bmatrix} r_0 \\ \theta_0 \end{bmatrix} + \begin{bmatrix} -\eta f(\theta_0) - \frac{\eta^2}{2} r_0 \frac{\partial f}{\partial \theta} + \mathcal{O}(\eta^3) - \eta C r_0 + \sqrt{2C\eta} w \\ \frac{\eta}{2} r_0 + \frac{\eta}{2} (r_0 - \eta f(\theta_0) - \eta C r_0 + \sqrt{2C\eta} w) + \mathcal{O}(\eta^3) \end{bmatrix} = \\ &= \begin{bmatrix} r_0 \\ \theta_0 \end{bmatrix} + \begin{bmatrix} \eta^{\frac{1}{2}} \sqrt{2C} w + \eta (-f(\theta_0) - C r_0) + \eta^2 (-\frac{1}{2} r_0 \frac{\partial f}{\partial \theta}) \\ \eta r_0 + \frac{\eta^{\frac{3}{2}}}{2} \sqrt{2C} w + \eta^2 (-\frac{1}{2} f(\theta_0) - \frac{1}{2} C r_0) \end{bmatrix} + \mathcal{O}(\eta^3) = \\ &= \begin{bmatrix} r_0 \\ \theta_0 \end{bmatrix} + \begin{bmatrix} \delta_r \\ \delta_\theta \end{bmatrix} + \mathcal{O}(\eta^3). \end{aligned}$$

Consequently, dropping the dependence on \mathbf{z}_0 (whenever unambiguous),

$$\begin{aligned} \phi(\mathbf{z}_1) &= \phi + \partial_r \phi \delta_r + \partial_\theta \phi \delta_\theta + \frac{\partial_{rr} \phi}{2} \delta_r^2 + \frac{\partial_{\theta\theta} \phi}{2} \delta_\theta^2 + \partial_{r\theta} \phi \delta_r \delta_\theta + \frac{\partial_{rrr} \phi}{6} \delta_r^3 + \frac{\partial_{\theta\theta\theta} \phi}{6} \delta_\theta^3 + \\ &+ \frac{3\partial_{rr\theta} \phi}{6} \delta_r^2 \delta_\theta + \frac{3\partial_{\theta\theta r} \phi}{6} \delta_\theta^2 \delta_r + \frac{\partial_{rrrr} \phi}{24} \delta_r^4 + \mathcal{O}(\eta^3). \end{aligned}$$

To derive the operator \mathcal{U} we need to take the expected value of both sides. We need the following equalities, that with an abuse of notation are valid up to $\mathcal{O}(\eta^3)$

$$\begin{aligned} \mathbb{E}(\delta_r) &= -\eta f - \frac{\eta^2}{2} r \partial_\theta f - \eta C r \\ \mathbb{E}(\delta_\theta) &= \eta r - \frac{\eta^2}{2} f - \frac{\eta^2}{2} C r \\ \mathbb{E}(\delta_r^2) &= \eta^2 C^2 r^2 + \eta^2 f^2 + 2\eta^2 C p f + 2\eta C \\ \mathbb{E}(\delta_\theta^2) &= \eta^2 r^2 \\ \mathbb{E}(\delta_r \delta_\theta) &= \eta^2 C + \eta^2 (-f r - C r^2) \\ \mathbb{E}(\delta_r^3) &= \eta^2 6C (-f - C r) \\ \mathbb{E}(\delta_\theta^3) &= 0 \\ \mathbb{E}(\delta_r^2 \delta_\theta) &= \eta^2 2C r \\ \mathbb{E}(\delta_\theta^2 \delta_r) &= 0 \\ \mathbb{E}(\delta_r^4) &= \eta^2 12C^2 \end{aligned}$$

By expanding the operator \mathcal{U} in powers of η we then obtain

$$\begin{aligned} \mathcal{U} = \mathbb{E}(\phi(z_1)) &= \phi + \eta \underbrace{((\partial_r \phi) (-f - C r) + (\partial_\theta \phi) r + (\partial_{rr} \phi) C)}_{\mathcal{L}} + \frac{\eta^2}{2} \underbrace{(-(\partial_r \phi) r \partial_\theta f - (\partial_\theta \phi) f - (\partial_\theta \phi) C r)}_{\mathcal{B}} \underbrace{+}_{\mathcal{F}} \underbrace{+}_{\mathcal{J}} \\ &+ \underbrace{(\partial_{rr} \phi) C^2 r^2}_{\mathcal{K}} + \underbrace{(\partial_{rr} \phi) f^2}_{\mathcal{G}} + \underbrace{(\partial_{rr} \phi) 2C r f}_{\mathcal{H}} + \underbrace{(\partial_{\theta\theta} \phi) r^2}_{\mathcal{A}} - \underbrace{2f r (\partial_{r\theta} \phi)}_{\mathcal{C}} - \underbrace{2C r^2 (\partial_{r\theta} \phi)}_{\mathcal{D}} + \underbrace{2C (\partial_{r\theta} \phi)}_{\mathcal{M}} \\ &\underbrace{- 2C f (\partial_{rrr} \phi)}_{\mathcal{I}} - \underbrace{2C^2 r (\partial_{rrr} \phi)}_{\mathcal{L}} + \underbrace{(\partial_{rr\theta} \phi) 2C r}_{\mathcal{E}} + \underbrace{(\partial_{rrrr} \phi) C^2}_{\mathcal{N}} + \mathcal{O}(\eta^3). \end{aligned} \quad (79)$$

The operator of interest is $\mathcal{L} = r\partial_\theta - f\partial_r - Cr\partial_r + C\partial_{rr}$. Expanding instead

$$\begin{aligned}
\mathcal{L}^2 &= (r\partial_\theta - f\partial_r - Cr\partial_r + C\partial_{rr})^2 = \\
&r\partial_\theta(r\partial_\theta - f\partial_r - Cr\partial_r + C\partial_{rr}) + \\
&- f\partial_r(r\partial_\theta - f\partial_r - Cr\partial_r + C\partial_{rr}) + \\
&- Cr\partial_r(r\partial_\theta - f\partial_r - Cr\partial_r + C\partial_{rr}) + \\
&C\partial_{rr}(r\partial_\theta - f\partial_r - Cr\partial_r + C\partial_{rr}) = \\
&\underbrace{r^2\partial_{\theta\theta}}_A - \underbrace{r\partial_\theta f\partial_r}_B - \underbrace{rf\partial_{r\theta}}_C - \underbrace{Cr^2\partial_{r\theta}}_D + \underbrace{Cr\partial_{rr\theta}}_E + \\
&\underbrace{-f\partial_\theta}_F - \underbrace{fr\partial_{r\theta}}_C + \underbrace{f^2\partial_{rr}}_G + \underbrace{fC\partial_r}_H + \underbrace{fCr\partial_{rr}}_I - \underbrace{fC\partial_{rrr}}_I + \\
&\underbrace{-Cr\partial_\theta}_J - \underbrace{Cr^2\partial_{r\theta}}_D + \underbrace{fCr\partial_{rr}}_H + \underbrace{C^2r\partial_r}_K + \underbrace{C^2r^2\partial_{rr}}_K - \underbrace{C^2r\partial_{rrr}}_L + \\
&\underbrace{2C\partial_{r\theta}}_M + \underbrace{Cr\partial_{rr\theta}}_E - \underbrace{fC\partial_{rrr}}_I - 2C^2\partial_{rr} - \underbrace{C^2r\partial_{rrr}}_L + \underbrace{C^2\partial_{rrrr}}_N
\end{aligned} \tag{80}$$

we see that not all the terms match the η^2 terms of the Taylor expansions of \mathcal{U} . As anticipated, it is not possible to state anything quantitatively precise, but noticing that many of the summands coincide provides an hint about the LEAPFROG performance.

As a side note, we stress moreover that the LEAPFROG scheme can be instead easily modified to be order-two at no additional computational cost, by leveraging the results of Eq. (70) and considering substituting the Euler step of Eq. (77) with the analytical one.

F Notes on previous results for high-order integrators

In this section we elaborate on some important differences between our work and the work in [9].

We remark that Theorem 4 in [9] is not aligned with the results we present in this work. Indeed, the work in [9] suggests that the only effects on the asymptotic invariant measure of an SG-MCMC algorithm are due to the order of the numerical integrators, independently of mini-batching.

Instead, our results in Theorem 3, show that an explicit bottleneck of order two is present due to mini-batches, i.e. due to the stochastic nature of gradient. The source of the inconsistency lies in the fact that while our two works share a set of assumptions, to ensure ergodicity of the dynamics and smoothness of the Kolmogorov differential equation, [9] requires some extra assumptions concerning the Poisson equation to prove the convergence rates. The formal justification of these extra assumptions, explicitly criticized in [30], has been deemed as out of the scope of [9].

In Appendix F.1, we present a simple toy example with known analytic solution, which contradicts the claims of [9], while our geometrical interpretation is compatible nevertheless. We consider an analytical integrator that corresponds to an arbitrarily high order numerical integration. We show that when considering mini-batches the stationary distribution is not the desired one, hinting at the presence of a bottleneck in accordance with our theory. Importantly, this is a different result from the one suggested in [9] where it is claimed that when considering mini-batches asymptotically in time, only the order of the numerical integrator determines the convergence rate.

Whether or not the assumptions of [9] for the solution of the Poisson equation hold for more complex models is left for future work. Not making them is the main difference with respect to our exposition, and is the source of difference for the theoretical results.

F.1 Toy example

In this section we introduce a toy example – whose dynamics has closed form solutions – to understand the role of mini-batching. For simplicity we consider a one dimensional case.

The prior distribution for the parameter θ is

$$p(\theta) = \mathcal{N}(\theta; 0, \sigma_\theta^2), \tag{81}$$

while the likelihood for any given observation is

$$p(x|\theta) = \mathcal{N}(x; \theta, \sigma_x^2), \quad (82)$$

where σ_θ, σ_x are arbitrary positive constants.

We consider the simplest case in which the dataset is composed by two datapoints, i.e. $N = 2$, $D = \{x_1, x_2\}$. Simple calculations show that the posterior distribution is of the form

$$p(\theta|D) = \mathcal{N}\left(\theta; \frac{x_1 + x_2}{v}, \sigma_l^2\right), \quad (83)$$

where $v = \frac{\sigma_x^2}{\sigma_\theta^2} + 2$ and $\sigma_l^2 = \left(\frac{1}{\sigma_\theta^2} + \frac{2}{\sigma_x^2}\right)^{-1}$.

The potential $U(\theta)$ corresponding to the distribution Eq. (83) has expression

$$U(\theta) = \frac{1}{2\sigma_l^2} \left(\theta - \left(\frac{x_1 + x_2}{v} \right) \right)^2 + \text{const.} \quad (84)$$

Notice that, up to constants of θ , the potential can be rewritten as

$$U(\theta) = \frac{1}{4\sigma_l^2} \left(\theta - \frac{2x_1}{v} \right)^2 + \frac{1}{4\sigma_l^2} \left(\theta - \frac{2x_2}{v} \right)^2. \quad (85)$$

Consequently the gradient has form

$$\nabla U(\theta) = \frac{1}{\sigma_l^2} \left(\theta - \frac{x_1 + x_2}{v} \right) = \frac{1}{2\sigma_l^2} \left(\theta - \frac{2x_1}{v} \right) + \frac{1}{2\sigma_l^2} \left(\theta - \frac{2x_2}{v} \right). \quad (86)$$

The potential and gradient with a sampled mini-batch corresponding to Eq. (85) and Eq. (86) are respectively

$$U_i(\theta) = \frac{1}{2\sigma_l^2} \left(\theta - \frac{2x_i}{v} \right)^2, \quad (87)$$

and

$$\nabla U_i(\theta) = \frac{1}{\sigma_l^2} \left(\theta - \frac{2x_i}{v} \right). \quad (88)$$

As shown in Appendix F.2, it is possible to build analytical integrators, that provide perfect simulation of paths. These integrators, that correspond to arbitrarily high order numerical integrators, are used for a numerical simulation with $\eta = 0.3$, $C = 2$, $\sigma_x^2 = 2$, $\sigma_\theta^2 = 0.5$ and two sampled datapoints $x_1 = 4$, $x_2 = -3.2$. The results, reported in Fig. 6, confirm our theory. Even considering a perfect integrator, when considering mini-batches, the stationary distribution is not the desired one. Importantly, this is a different result from the one suggested in [9] where it is claimed that asymptotically in time only the order of the numerical integrator determines the convergence rate.

We further support our numerical evidence with a thorough theoretical exploration in Appendix F.2.

F.2 Derivation of the analytical integrators

We consider the dynamics of Eq. (3), where for simplicity $\mathbf{M} = 1$. We then have, remembering $\mathbf{z}(t) = \begin{bmatrix} r(t) \\ \theta(t) \end{bmatrix}$, the following SDE

$$d\mathbf{z}(t) = \begin{bmatrix} -C & -1 \\ 1 & 0 \end{bmatrix} \begin{bmatrix} r(t) \\ \sigma_l^{-2}(\theta(t) - \frac{x_1 + x_2}{v}) \end{bmatrix} dt + \begin{bmatrix} \sqrt{2C}dw(t) \\ 0 \end{bmatrix}, \quad (89)$$

that we rewrite in the more convenient form

$$d\mathbf{z}(t) = \begin{bmatrix} -C & -\sigma_l^{-2} \\ 1 & 0 \end{bmatrix} \left(\mathbf{z}(t) - \begin{bmatrix} 0 \\ \bar{x} \end{bmatrix} \right) dt + \begin{bmatrix} \sqrt{2C}dw(t) \\ 0 \end{bmatrix}, \quad (90)$$

where $\bar{x} = \frac{x_1 + x_2}{v}$.

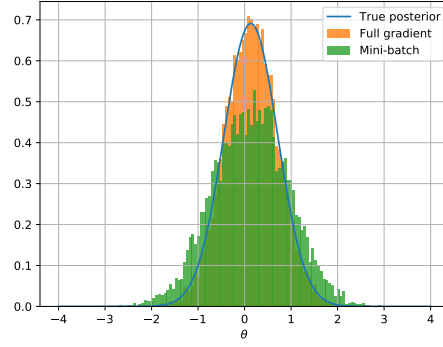


Figure 6: Histograms of stationary distributions

Starting from initial conditions $\mathbf{z}(0) = \mathbf{z}_0$, with calculations similar to Appendix E.1, we can shown that the system has analytic solution

$$\mathbf{z}(t) = \exp(t\mathbf{A}) \left(\mathbf{z}_0 - \begin{bmatrix} 0 \\ \bar{x} \end{bmatrix} \right) + \begin{bmatrix} 0 \\ \bar{x} \end{bmatrix} + \int_{s=0}^t \exp((t-s)\mathbf{A}) \begin{bmatrix} \sqrt{2C}dw(s) \\ 0 \end{bmatrix} \quad (91)$$

where for simplicity we have defined $\mathbf{A} = \begin{bmatrix} -C & -\sigma_l^{-2} \\ 1 & 0 \end{bmatrix}$. Considering that $\sigma_l^{-2}, C > 0$ simple calculations show that the eigenvalues of \mathbf{A} have negative real part, ensuring that as $t \rightarrow \infty$ we have $\exp(t\mathbf{A}) \rightarrow \mathbf{0}$.

A probabilistically equivalent representation of eq. Eq. (91) is the following

$$\mathbf{z}(t) = \exp(t\mathbf{A}) \left(\mathbf{z}_0 - \begin{bmatrix} 0 \\ \bar{x} \end{bmatrix} \right) + \begin{bmatrix} 0 \\ \bar{x} \end{bmatrix} + \mathbf{n}, \quad (92)$$

where

$$\mathbf{n} \sim \mathcal{N} \left(\mathbf{0}, \int_{s=0}^t \exp((t-s)\mathbf{A}) \begin{bmatrix} 2C & 0 \\ 0 & 0 \end{bmatrix} \exp((t-s)\mathbf{A}^\top) ds \right). \quad (93)$$

Equation Eq. (92) guarantees that it is possible to build a numerical integrator for any chosen step size η that simulates exactly the dynamics, corresponding to an arbitrarily high order of weak integration.

Convergence to the posterior

We then explore the transition probability starting from a given initial state \mathbf{z}_0 induced by such a numerical integrator with step size η

$$p(\mathbf{z}(\eta)|\mathbf{z}(0) = \mathbf{z}_0) = \mathcal{N} \left(\mathbf{z}(\eta); \exp(\eta\mathbf{A}) \left(\mathbf{z}_0 - \begin{bmatrix} 0 \\ \bar{x} \end{bmatrix} \right) + \begin{bmatrix} 0 \\ \bar{x} \end{bmatrix}, \int_{s=0}^{\eta} \exp((\eta-s)\mathbf{A}) \begin{bmatrix} 2C & 0 \\ 0 & 0 \end{bmatrix} \exp((\eta-s)\mathbf{A}^\top) ds \right). \quad (94)$$

As shown in Appendix F.2.1, the covariance matrix of the distribution Eq. (94) can be expressed as

$$\int_{s=0}^{\eta} \exp((\eta-s)\mathbf{A}) \begin{bmatrix} 2C & 0 \\ 0 & 0 \end{bmatrix} \exp((\eta-s)\mathbf{A}^\top) ds = \begin{bmatrix} 1 & 0 \\ 0 & \sigma_l^2 \end{bmatrix} - \exp(\eta\mathbf{A}) \begin{bmatrix} 1 & 0 \\ 0 & \sigma_l^2 \end{bmatrix} \exp(\eta\mathbf{A}^\top), \quad (95)$$

and consequently, we can rewrite Eq. (94) as

$$p(\mathbf{z}(\eta)|\mathbf{z}(0) = \mathbf{z}_0) = \mathcal{N}\left(\mathbf{z}(\eta); \exp(\eta\mathbf{A})\left(\mathbf{z}_0 - \begin{bmatrix} 0 \\ \bar{x} \end{bmatrix}\right) + \begin{bmatrix} 0 \\ \bar{x} \end{bmatrix}, \Sigma(\eta)\right), \quad (96)$$

where we introduced the $\Sigma(\eta) = \begin{bmatrix} 1 & 0 \\ 0 & \sigma_l^2 \end{bmatrix} - \exp(\eta\mathbf{A}) \begin{bmatrix} 1 & 0 \\ 0 & \sigma_l^2 \end{bmatrix} \exp(\eta\mathbf{A}^\top)$.

Importantly, we have that $\rho_{ss}(\mathbf{z})$ is the stationary distribution of the stochastic process, if and only if the following holds:

$$\rho_{ss}(\mathbf{z}^*) = \int p(\mathbf{z}(\eta) = \mathbf{z}^*|\mathbf{z}(0) = \mathbf{z})\rho_{ss}(\mathbf{z})d\mathbf{z} \quad (97)$$

where obviously the equality must hold for all η . To check that eq. Eq. (97) holds with:

$$\rho_{ss}(\mathbf{z}) = \mathcal{N}(r; 0, 1)\mathcal{N}\left(\theta; \frac{x_1 + x_2}{v}, \sigma_l^2\right) = \mathcal{N}\left(\mathbf{z}; \begin{bmatrix} 0 \\ \bar{x} \end{bmatrix}, \begin{bmatrix} 1 & 0 \\ 0 & \sigma_l^2 \end{bmatrix}\right) \quad (98)$$

we substitute directly:

$$\begin{aligned} & \int p(\mathbf{z}(\eta) = \mathbf{z}^*|\mathbf{z}(0) = \mathbf{z})\rho_{ss}(\mathbf{z})d\mathbf{z} = \\ & \int \mathcal{N}\left(\mathbf{z}^*; \exp(\eta\mathbf{A})\left(\mathbf{z} - \begin{bmatrix} 0 \\ \bar{x} \end{bmatrix}\right) + \begin{bmatrix} 0 \\ \bar{x} \end{bmatrix}, \Sigma(\eta)\right) \mathcal{N}\left(\mathbf{z}; \begin{bmatrix} 0 \\ \bar{x} \end{bmatrix}, \begin{bmatrix} 1 & 0 \\ 0 & \sigma_l^2 \end{bmatrix}\right) d\mathbf{z} \\ & = \mathcal{N}\left(\mathbf{z}^*; \exp(\eta\mathbf{A})\left(\begin{bmatrix} 0 \\ \bar{x} \end{bmatrix} - \begin{bmatrix} 0 \\ \bar{x} \end{bmatrix}\right) + \begin{bmatrix} 0 \\ \bar{x} \end{bmatrix}, \Sigma(\eta) + \exp(\eta\mathbf{A}) \begin{bmatrix} 1 & 0 \\ 0 & \sigma_l^2 \end{bmatrix} \exp(\eta\mathbf{A}^\top)\right) \\ & = \mathcal{N}\left(\mathbf{z}^*; \begin{bmatrix} 0 \\ \bar{x} \end{bmatrix}, \begin{bmatrix} 1 & 0 \\ 0 & \sigma_l^2 \end{bmatrix}\right) \end{aligned}$$

proving that the stationary distribution is indeed the desired one.

Failure of convergence in the case of mini-batches

In the following, we show that when considering mini-batches instead, we fail to converge to the true posterior. Importantly this is true even with the analytical solution for the steps of the integrator, stressing that numerical integration and mini-batching have two independent effects. With mini-batches, at every step of the integration a x_1, x_2 are sampled with probability $\frac{1}{2}$.

Instead of simulating eq. Eq. (90) at every step of the numerical integration, the following stochastic process is then considered:

$$d\mathbf{z}(t) = \begin{bmatrix} -C & -\sigma_l^{-2} \\ 1 & 0 \end{bmatrix} \left(\mathbf{z}(t) - \begin{bmatrix} 0 \\ \bar{x}_i \end{bmatrix}\right) dt + \begin{bmatrix} \sqrt{2C}dw(t) \\ 0 \end{bmatrix} \quad (99)$$

where, $\bar{x}_i = \frac{2x_i}{v}$, and $i = 1$ or $i = 2$ is sampled randomly.

Similarly to the previous case it is possible to construct a numerical integrator that solves exactly the dynamics, this time with the potential computed using randomly only one of the two datapoints. The transition probability induced by such an integrator will then be equal to:

$$\begin{aligned} p(\mathbf{z}(\eta) = \mathbf{z}^*|\mathbf{z}(0) = \mathbf{z}_0) &= \frac{1}{2}\mathcal{N}\left(\mathbf{z}^*; \exp(\eta\mathbf{A})\left(\mathbf{z}_0 - \begin{bmatrix} 0 \\ \bar{x}_1 \end{bmatrix}\right) + \begin{bmatrix} 0 \\ \bar{x}_1 \end{bmatrix}, \Sigma(\eta)\right) \\ &+ \frac{1}{2}\mathcal{N}\left(\mathbf{z}^*; \exp(\eta\mathbf{A})\left(\mathbf{z}_0 - \begin{bmatrix} 0 \\ \bar{x}_2 \end{bmatrix}\right) + \begin{bmatrix} 0 \\ \bar{x}_2 \end{bmatrix}, \Sigma(\eta)\right) \end{aligned} \quad (100)$$

$$= \frac{1}{2}f_1(\mathbf{z}^*, \eta, \mathbf{z}_0) + \frac{1}{2}f_2(\mathbf{z}^*, \eta, \mathbf{z}_0), \quad (101)$$

where f_1, f_2 are the two Gaussian transition probabilities. Importantly, this allows to state the following central statement: the distribution $p(\theta|\mathcal{D})$ is not the stationary distribution of the process. This claim can be proven by contradiction. Suppose that the stationary distribution is the one of

interest, $\mathcal{N}\left(\mathbf{z}; \begin{bmatrix} 0 \\ \bar{x} \end{bmatrix}, \begin{bmatrix} 1 & 0 \\ 0 & \sigma_l^2 \end{bmatrix}\right)$. Performing one step of integration the new distribution will be of the form:

$$\rho_{new}(\mathbf{z}^*) = \int \left(\frac{1}{2} f_1(\mathbf{z}^*, \eta, \mathbf{z}) + \frac{1}{2} f_2(\mathbf{z}^*, \eta, \mathbf{z}) \right) \rho_{ss}(\mathbf{z}) d\mathbf{z} \quad (102)$$

$$\begin{aligned} &= \frac{1}{2} \mathcal{N}\left(\mathbf{z}^*; \exp(\eta \mathbf{A}) \left(\begin{bmatrix} 0 \\ \bar{x} \end{bmatrix} - \begin{bmatrix} 0 \\ \bar{x}_1 \end{bmatrix} \right) + \begin{bmatrix} 0 \\ \bar{x} \end{bmatrix}, \begin{bmatrix} 1 & 0 \\ 0 & \sigma_l^2 \end{bmatrix}\right) \\ &+ \frac{1}{2} \mathcal{N}\left(\mathbf{z}^*; \exp(\eta \mathbf{A}) \left(\begin{bmatrix} 0 \\ \bar{x} \end{bmatrix} - \begin{bmatrix} 0 \\ \bar{x}_2 \end{bmatrix} \right) + \begin{bmatrix} 0 \\ \bar{x} \end{bmatrix}, \begin{bmatrix} 1 & 0 \\ 0 & \sigma_l^2 \end{bmatrix}\right) \\ &\neq \rho_{ss}(\mathbf{z}^*). \end{aligned} \quad (103)$$

By definition, we should have the functional equivalence between ρ_{new} and ρ_{ss} . Equation Eq. (102) implies however that after the mixture transition probability the new density ρ_{new} will be a mixture of Gaussian distributions, and consequently $\rho_{new} \neq \rho_{ss}$. This concludes the demonstration that the stationary distribution is not the one of interest.

F.2.1 Derivation of eq. Eq. (95)

Define:

$$\mathbf{K}(t) = \int_{s=0}^t \exp((t-s)\mathbf{A}) \begin{bmatrix} 2C & 0 \\ 0 & 0 \end{bmatrix} \exp((t-s)\mathbf{A}^\top) ds, \quad (105)$$

and

$$\mathbf{S}(t) = \begin{bmatrix} 1 & 0 \\ 0 & \sigma_l^2 \end{bmatrix} - \exp(t\mathbf{A}) \begin{bmatrix} 1 & 0 \\ 0 & \sigma_l^2 \end{bmatrix} \exp(t\mathbf{A}^\top). \quad (106)$$

Immediately we see that $\mathbf{K}(0) = \mathbf{S}(0) = \mathbf{0}$.

The derivative of $\mathbf{K}(t)$ has expression:

$$\begin{aligned} \frac{d\mathbf{K}(t)}{dt} &= \exp((t-t)\mathbf{A}) \begin{bmatrix} 2C & 0 \\ 0 & 0 \end{bmatrix} \exp((t-t)\mathbf{A}^\top) \\ &+ \mathbf{A} \int_{s=0}^t \exp((t-s)\mathbf{A}) \begin{bmatrix} 2C & 0 \\ 0 & 0 \end{bmatrix} \exp((t-s)\mathbf{A}^\top) ds \\ &+ \int_{s=0}^t \exp((t-s)\mathbf{A}) \begin{bmatrix} 2C & 0 \\ 0 & 0 \end{bmatrix} \exp((t-s)\mathbf{A}^\top) ds \mathbf{A}^\top \\ &= \begin{bmatrix} 2C & 0 \\ 0 & 0 \end{bmatrix} + \mathbf{A}\mathbf{K}(t) + \mathbf{K}(t)\mathbf{A}^\top. \end{aligned}$$

Similarly we have:

$$\begin{aligned} \frac{d\mathbf{S}(t)}{dt} &= -\mathbf{A} \exp(t\mathbf{A}) \begin{bmatrix} 1 & 0 \\ 0 & \sigma_l^2 \end{bmatrix} \exp(t\mathbf{A}^\top) - \exp(t\mathbf{A}) \begin{bmatrix} 1 & 0 \\ 0 & \sigma_l^2 \end{bmatrix} \exp(t\mathbf{A}^\top) \mathbf{A}^\top \\ &= -\mathbf{A} \left(\begin{bmatrix} 1 & 0 \\ 0 & \sigma_l^2 \end{bmatrix} - \mathbf{S}(t) \right) - \left(\begin{bmatrix} 1 & 0 \\ 0 & \sigma_l^2 \end{bmatrix} - \mathbf{S}(t) \right) \mathbf{A}^\top. \end{aligned}$$

Since $\mathbf{A} \begin{bmatrix} 1 & 0 \\ 0 & \sigma_l^2 \end{bmatrix} = \begin{bmatrix} -C & -1 \\ 1 & 0 \end{bmatrix}$, we can prove

$$\frac{d\mathbf{S}(t)}{dt} = \begin{bmatrix} 2C & 0 \\ 0 & 0 \end{bmatrix} + \mathbf{A}\mathbf{S}(t) + \mathbf{S}(t)\mathbf{A}^\top.$$

Defining the difference matrix $\mathbf{H}(t) = \mathbf{K}(t) - \mathbf{S}(t)$ we recognize that it satisfies the differential equation

$$\frac{d\mathbf{H}(t)}{dt} = \mathbf{A}\mathbf{H}(t) + \mathbf{H}(t)\mathbf{A}^\top$$

that has explicit solution

$$\mathbf{H}(t) = \exp(t\mathbf{A}) \mathbf{H}(0) \exp(t\mathbf{A}^\top) \quad (107)$$

Since $\mathbf{H}(0) = \mathbf{0}$ we conclude $\mathbf{H}(t) = \mathbf{0}$ proving the desired equality.

G Experiments: Additional details

G.1 Experimental setup

Throughout our experimental campaign, we work on a number of datasets from the UCI repository³. For each dataset, we have considered 5 random splits into training and test sets; for the regression datasets, we have adopted the splits in [38] which are available online⁴ under the Creative Commons licence. The primary point of interest in this work is the predictive distribution over the test set and how this deviates from the true posterior. Table 1 and Table 2 summarize the details of the regression and classification datasets in this work. In the same tables we report some error metrics; the latter are not a central part of the evaluation of this paper, but they are simply indicative of the performance of SHMC. Our implementation is loosely based on the PYSGMCMC framework⁵.

Network architecture. Throughout this experimental campaign, we consider BNNs featuring L layers, where each layer is defined as follows:

$$f_l(\mathbf{x}) = \frac{1}{\sqrt{D_{l-1}}} \mathbf{W}_l \varphi(f_{l-1}(\mathbf{x})) + \mathbf{b}_l, \quad l \in \{1, \dots, L+1\}, \quad (108)$$

where φ is a non-linear activation function. The model parameters are summarized as $\theta \equiv \{\mathbf{W}_l \in \mathbb{R}^{D_l \times D_{l-1}}, \mathbf{b}_l \in \mathbb{R}^{D_l \times 1}\}$, and they denote the matrix of weights and the vector of biases for layer l . Note that we divide by the square root of the input dimension D_{l-1} ; this scheme is known as the *NTK parameterization* [26; 28], and it ensures that the asymptotic variance neither explodes nor vanishes. In this context, we place a standard Gaussian prior for both weights and biases, i.e. $p(\theta) = \mathcal{N}(0, I)$.

Regression and classification tasks. For regression tasks we consider BNNs with 4 layers and 50 nodes per layer with RELU activation. Table 1 outlines the predictive performance of SHMC for four regression datasets (BOSTON, CONCRETE, ENERGY and YACHT), as well as the noise variance σ^2 used in each case. We have drawn 200 samples from the posterior and the regression performance is evaluated in terms of *root mean squared error* (RMSE) and *mean negative log-likelihood* MNLL. In order to put these values into perspective, we also show the results for the adaptive SGHMC scheme from [44] featuring a network of identical structure as in our setup. In both cases, the full-batch gradient was used.

Table 1: Regression results for BNNs with 4 layers and 50 nodes per layer with RELU activation.

DATASET	Training Size	Test Size	σ^2	Test RMSE(\downarrow)		Test MNLL(\downarrow)	
				SHMC	SGHMC [44]	SHMC	SGHMC [44]
Boston	455	51	0.2	2.821 \pm 0.61	2.825 \pm 0.63	2.600 \pm 0.09	2.600 \pm 0.09
Concrete	927	103	0.05	4.907 \pm 0.39	4.833 \pm 0.46	2.971 \pm 0.07	2.948 \pm 0.09
Energy	691	77	0.01	0.501 \pm 0.07	0.489 \pm 0.07	1.191 \pm 0.07	1.120 \pm 0.03
Yacht	277	31	0.005	0.420 \pm 0.12	0.436 \pm 0.13	1.180 \pm 0.02	1.176 \pm 0.02

For classification we consider IONOSPHERE and VEHICLE from UCI, for which we sample from RELU BNNs with 2 layers and 50 nodes per layer. We have drawn 200 samples from the posterior, and the predictive accuracy and test MNLL of SHMC can be seen in Table 2, where we also show the performance of the adaptive version of SGHMC [44]. The results have been very similar for these two cases; this has been expected, as both methods are supposed to converge to the same posterior.

³<https://archive.ics.uci.edu/ml/index.php>

⁴<https://github.com/yaringal/DropoutUncertaintyExps>

⁵<https://github.com/MFreidank/pysgmcmc>

Table 2: Classification results for BNNs with 2 layers and 50 nodes per layer with RELU activation.

DATASET	Classes	Training Size	Test Size	Test accuracy(\uparrow)		Test MNLL(\downarrow)	
				SHMC	SGHMC [44]	SHMC	SGHMC [44]
Ionosphere	2	301	34	0.920 ± 0.03	0.916 ± 0.02	0.294 ± 0.04	0.295 ± 0.04
Vehicle	4	646	200	0.777 ± 0.02	0.783 ± 0.02	0.588 ± 0.03	0.588 ± 0.03

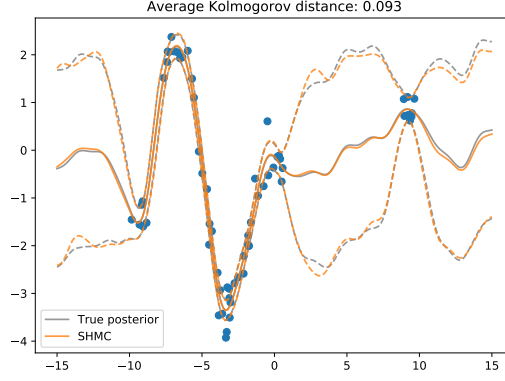


Figure 7: True and SHMC predictive posterior on a synthetic dataset.

Synthetic regression example. We also consider as simple regression model applied on the synthetic one-dimensional dataset of Fig. 7. In this case we choose a linear model with fixed basis functions, in order to demonstrate SHMC convergence in a fully controlled environment where the true posterior can be calculated analytically. We consider $D = 256$ trigonometric basis functions: $f(x) = \sqrt{2/D} \mathbf{w}^\top \cos(\omega x - \pi/4)$, where $\mathbf{w} \in \mathbb{R}^{D \times 1}$ contains the weights of D features and $\omega \in \mathbb{R}^{D \times 1}$ is a vector of fixed frequencies. In the experiments that follow, we have a Gaussian likelihood with variance 0.1 and prior $p(\mathbf{w}) = \mathcal{N}(0, I_D)$. The predictive posterior can be seen in Fig. 7, where the test set consists of 200 uniformly distributed points.

G.2 Comparison framework and convergence to posterior

Comparing predictive distributions. In this work, we explore the behavior of a number of methods by comparing the predictive distribution given by a particular setting to the distribution of an oracle. The comparison is performed in terms of one-dimensional predictive marginals using 200 samples: for each test point we evaluate the Kolmogorov distance between the predictive distribution and the oracle. We then report the average distance over the test set. The Kolmogorov distance takes values between 0 and 1. In Fig. 7 we show an one-dimensional regression example where the average distance values over the test set is smaller than 0.1.

Self-distance. When we compare the distance between empirical distribution, this will never be exactly zero. In order to determine whether a given sample is a sufficiently good approximation for a target distribution, we have to compare the corresponding distance value to the *self-distance*. The latter can be evaluated by resampling from the oracle posterior distribution: for each oracle we consider 5 independent runs producing 200 samples each, which are used to estimate the Kolmogorov self-distance. In the results of Fig. 8, Fig. 9, Fig. 10 and Fig. 11, the shaded area denotes the 0.05 and 0.95-quantiles of the self-distance distribution.

Methods summary. The main focus of this experimental campaign is to explore how SHMC is affected by changes of step size and batch size. For SHMC, we consider 4 integrators of different properties: EULER, LEAPFROG, RK2 and LIE-TROTTER, and we investigate whether its behavior differs from HMC and SGHMC [10]. We also compare against the symmetric splitting integrator proposed in [9], which we refer to as SYMMETRIC.

Computational summary. At this point, we note that each block in Fig. 8, Fig. 9, Fig. 10 and Fig. 11 corresponds to 5 random splits or seeds. For most datasets, drawing 200 samples for the smallest step size (i.e. 0.001) required 15–20 minutes. Such a small step size has been necessary in order to demonstrate convergence for small batch sizes. A full exploration of the methods and integrators for a single split (or seed) of a single dataset required approximately one day of computation on a computer cluster featuring Intel® Xeon® CPU @2.00GHz. It has not been possible to do this kind of exploration in a meaningful way for larger datasets, yet we believe that the existing results are sufficient to demonstrate our theoretical claims.

Convergence. In order to reason about convergence in the experiments that follow, we have taken great care to approximate the true posterior with SGHMC, which we treat as oracle. For the oracles we consider full-batch and $\eta = 0.005$ in all cases, except for the linear model where the true posterior has been analytically tractable. The simulation time has been determined by adjusting the thinning parameter so that lag-1 autocorrelation ($\text{ACF}(1)$) was considered as acceptable. In practice we keep one sample every 500 steps (i.e. thinning), and we discard the first 2000 steps. Then for each oracle, the simulation time was doubled one more time, but that resulted in no significant difference in the predictive distribution. The summary of $\text{ACF}(1)$ values that correspond to the oracles used in this work can be found in Table 3. As a final remark, we note that for each combination of dataset and model, all random walks cover the same simulation time. The CPU time is thus determined by the step size η : a larger value for η implies that a smaller number of steps is required to simulate a certain system, as the thinning parameter is adjusted accordingly. In the case of HMC, we choose the integration length to match the thinning parameter, so that is it given the same computational budget as the rest of the methods.

Table 3: Lag 1 autocorrelation for the SGHMC algorithms used as oracles.

DATASET	ACF(1)
Boston	0.09
Concrete	0.23
Energy	0.05
Yacht	0.05
Ionosphere	0.17
Vehicle	0.18

G.3 Extended regression and classification results

In this section we present the results of step size and batch size exploration for the entirety of datasets considered.

Comparing SHMC with sampling methods. Figure 8 focuses on the comparison between SHMC (with LEAPFROG integrator) and other methods from the literature, including HMC, SGHMC and SYMMETRIC. For all cases except HMC, we set $C = 5$; we find this to be a reasonable choice, as we see in the exploration of Appendix G.4. We see that for almost all datasets, there is not significant difference among LEAPFROG, SGHMC and SYMMETRIC; all three methods respond in a very similar way to the changes of both the step size and the batch size. We note that SHMC (LEAPFROG) is different from SGHMC in the sense that no counterbalancing of the noise is performed by the former. We think that this result is compatible with our position that counterbalancing the gradient noise is not necessary to sample from the posterior.

Regarding the behavior of HMC, we see that in some cases (i.e. BOSTON, IONOSPHERE, VEHICLE) the algorithm seems to converge the true posterior as the step size approaches 0. We can also see however that the curve of HMC raises significantly faster than the other methods as the step size grows. We believe that this difference reflects our theoretical discussion in Section 4.

We stress that that HMC has been given exactly the same computational budget and hyperparameters (step size, integration length) as the rest of the methods in this comparison. Although it is possible to obtain better results by carefully tuning [40; 23], our priority has been to demonstrate the difference in convergence.

Comparing SHMC integrators. The results for several SHMC integrators for $C = 5$ can be found in Fig. 9. First of all, it is easy to see that EULER is not competitive; it requires substantially smaller steps sizes in order to approximate the desired posterior.

It is worth also commenting on the performance of RK2: although it is mostly comparable to the symplectic integrators (i.e. LEAPFROG, LIE-TROTTER), it seems to be less stable in some cases. This is more visible in the fourth column of Fig. 9 (i.e. full-batch) for the datasets: BOSTON, CONCRETE, ENERGY and YACHT. In these cases, some larger step sizes for RK2 do not converge to the true posterior. The benefits of symplectic integrators are very well-known in the literature, and our results are in line with this common knowledge.

Perhaps somewhat surprisingly, we observed no significant difference between LEAPFROG and LIE-TROTTER, despite the fact that LEAPFROG is provably only of order 1. In fact, LEAPFROG has been competitive to order-2 schemes (LIE-TROTTER, SYMMETRIC, RK2) in most of our experiments. We think that this behavior is due to the fact that most of the terms of its Taylor expansion cancel out, as we show in Appendix E. In practice, this means that LEAPFROG is a very sensible choice for SHMC. We stress that this position refers to our sampling case study, where ergodic convergence is of interest only. These findings should not be generalized to cases where either weak or strong convergence is desirable.

G.4 Exploration of the friction constant C

The user-specified constant C appears twice in Eq. (3): in the friction term and in the stochastic diffusion term of the SDE. Although Theorem 1 implies that any choice for $C > 0$ will maintain the desired stationary distribution (i.e. $\rho_{ss}(\theta) \propto \exp(-U(\theta))$), the transient dynamics of the SDE do change as we have seen in the sample paths of Fig. 1. It is generally expected that as C approaches 0, the sample paths approach the deterministic behavior of an ODE. On the other hand, if C is too large, the stochastic process degenerates to the standard Brownian motion. It is expected that either of these extremes would hurt the usability of SDE simulation as a sampling scheme, but the exact effect of C is not apparent.

In this section, we experimentally examine how a certain choice for C affects practical convergence to the desired posterior in conjunction with the step size η as well as the mini-batch size. Figure 10 summarizes an extensive exploration of C for all the models and datasets considered in this work using the LEAPFROG integrator, with C varying from 0.5 to 100. Again, we measure the average Kolmogorov distance from the true predictive posterior for the test points, and we want to see whether the curve for varying η and batch size approaches the band of self-distance.

As a general remark, the desired convergence properties are not too sensitive to the constant C . Although, the optimal value for C does depend on the dynamics induced by a particular dataset and model, it appears that there is a wide range of values that can be considered as acceptable. For most of the cases considered, a value between 5 and 10 seems to produce reasonable results. Nevertheless, we think that some manual exploration would still be required for a new dataset.

G.5 Exploration in a preconditioning setting.

Here we perform an exploration of the effects of a non-scalar form for C . More specifically, we consider C to be a diagonal matrix, which is implicitly defined through the mass matrix \mathbf{M} and the scalar constant $c_{\mathbf{M}} = C\mathbf{M}^{-1}$. For the largest part of the experimental campaign, we have considered a mass matrix equal to the identity, but any symmetric, positive definite mass matrix is a valid choice. In this experiment, we consider a diagonal form for $\mathbf{M} = \tilde{\mathbf{V}}$, where $\tilde{\mathbf{V}}$ contains the estimated variances of the gradient over a moving average window during a pre-simulation phase, as described in [44]. We use the LEAPFROG integrator, but in contrast with [44], we do not do any counterbalancing of the gradient noise. In both cases, the full-batch gradient was used.

The results for varying $c_{\mathbf{M}} = C\mathbf{M}^{-1}$ from 0.5 to 100 can be found in Fig. 11. Similar to the previous experiment, only the transient SDE dynamics are modified, while the steady-state behavior remains unchanged. We see that except for some values for $c_{\mathbf{M}}$ that are too large (i.e. > 10), the exploration yields results that converge more reliably to the desired posterior compared to the setting of scalar C exploration in Fig. 10. We argue that this is a sensible strategy to automatically tune the friction term, as the scheme constitutes a kind of preconditioning: the gradient components with high

variability will be associated with smaller step sizes. In conclusion, we think that a modification of the dynamics as in [44] may significantly improve usability for SDE-based sampling, as larger step sizes are admissible.

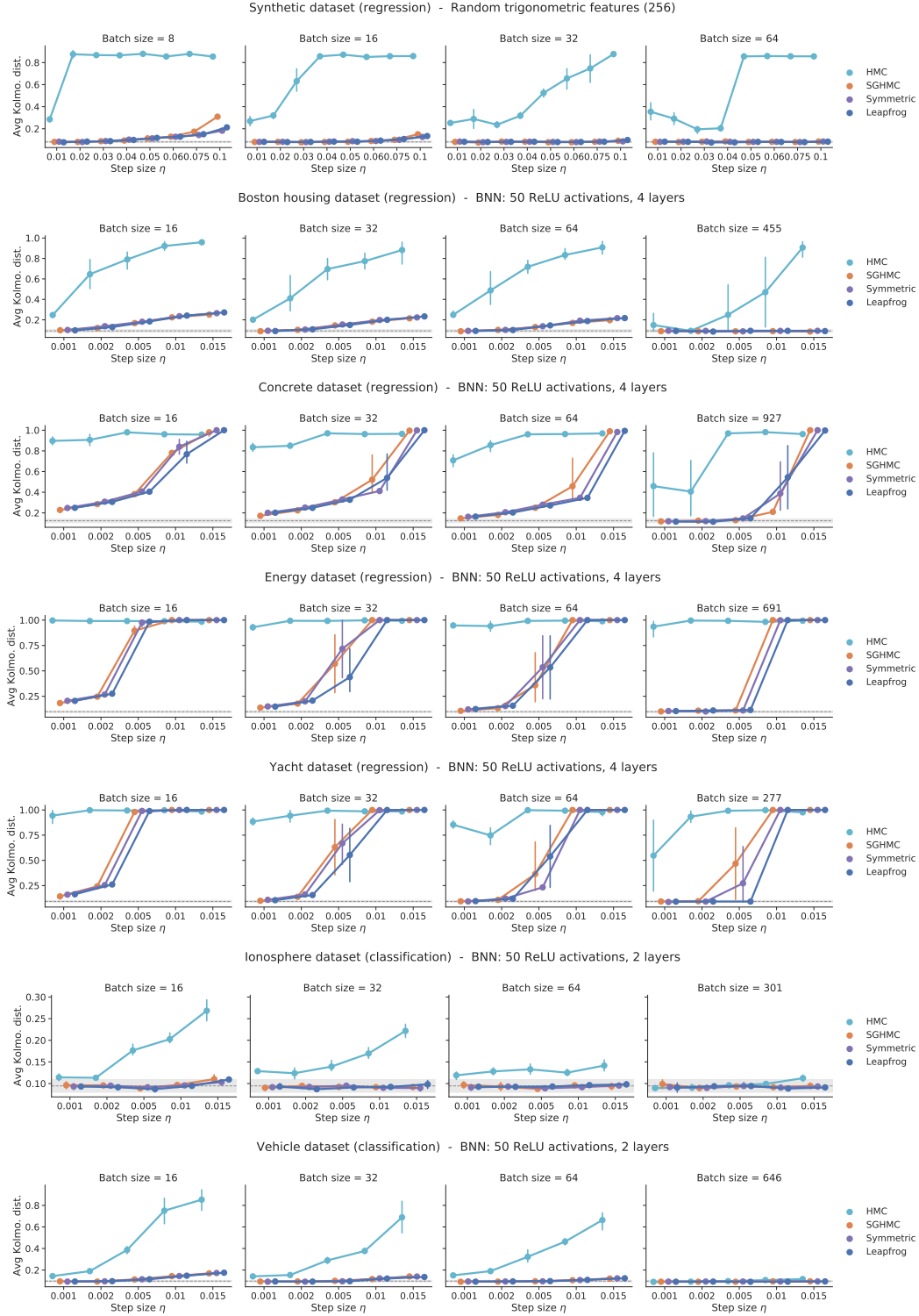


Figure 8: Exploration of step size and batch size for different Hamiltonian-based methods; the grey dotted line denotes the self-distance for the distribution of the oracle. The standard HMC cannot compete with SDE-based methods given the computational budget, as careful tuning of the integration length is required. The rest of the methods have similar behavior; the noise counterbalancing of SGHMC does not seem to offer any improvement regarding the posterior approximation.

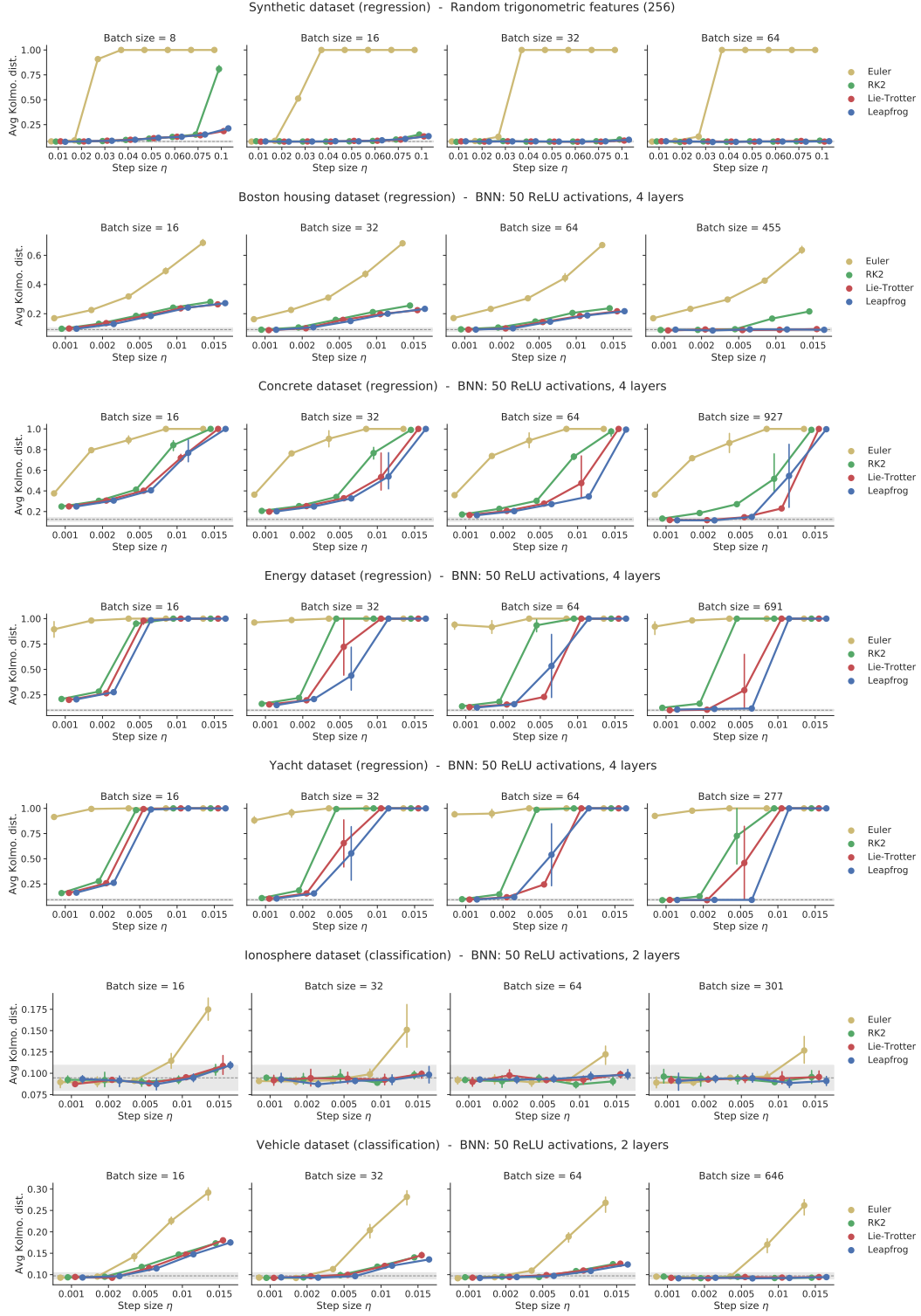


Figure 9: Exploration of step size and batch size for different SDE-HMC integrators; the grey dotted line denotes the self-distance for the distribution of the oracle. Notice that leapfrog behaves as a second order integrator, although it is provably only first order.

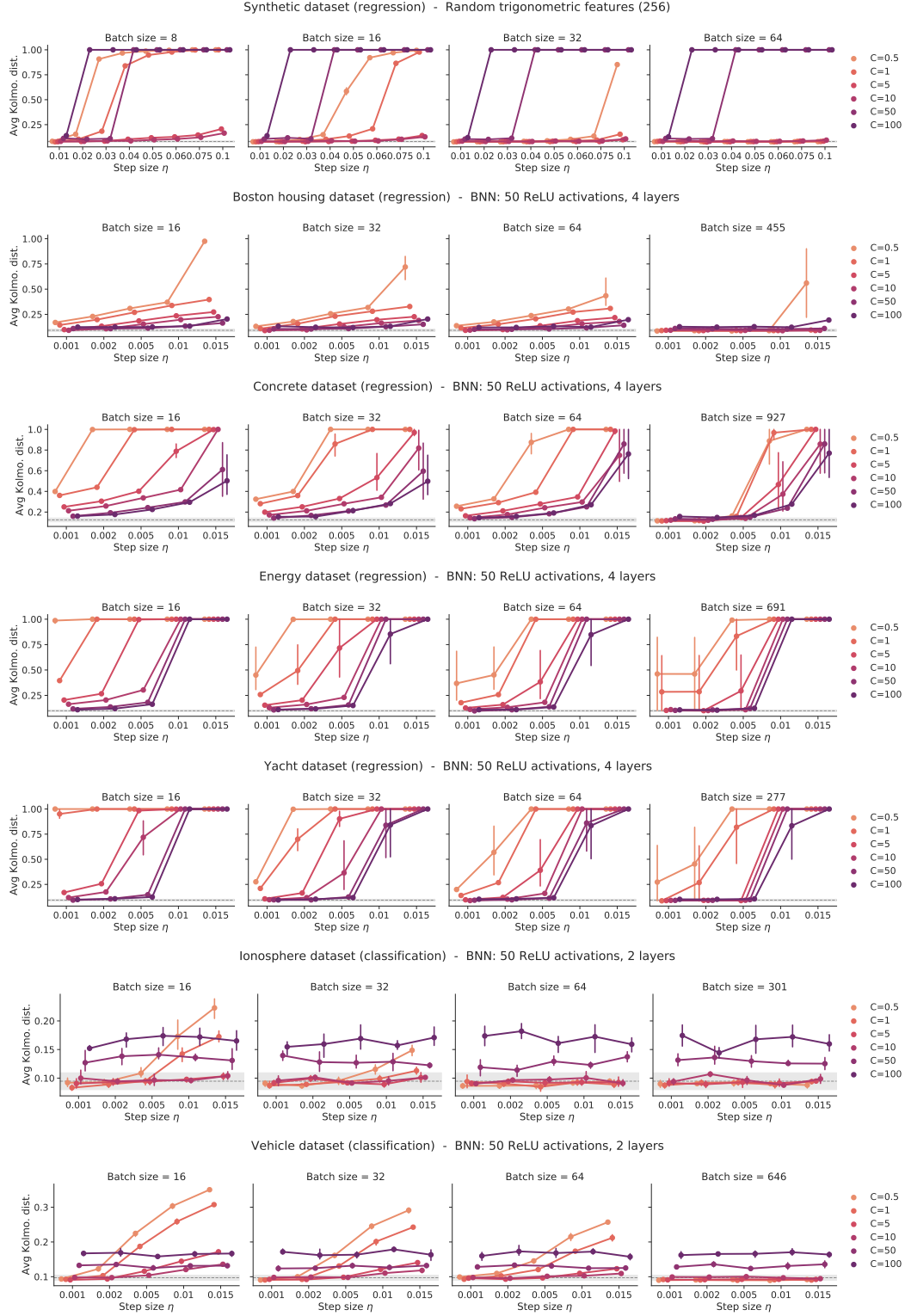


Figure 10: Exploration of step size and batch size for different values of a scalar friction coefficient C . The grey dotted line denotes the self-distance for the distribution of the oracle. The LEAPFROG integrator is used in all cases.

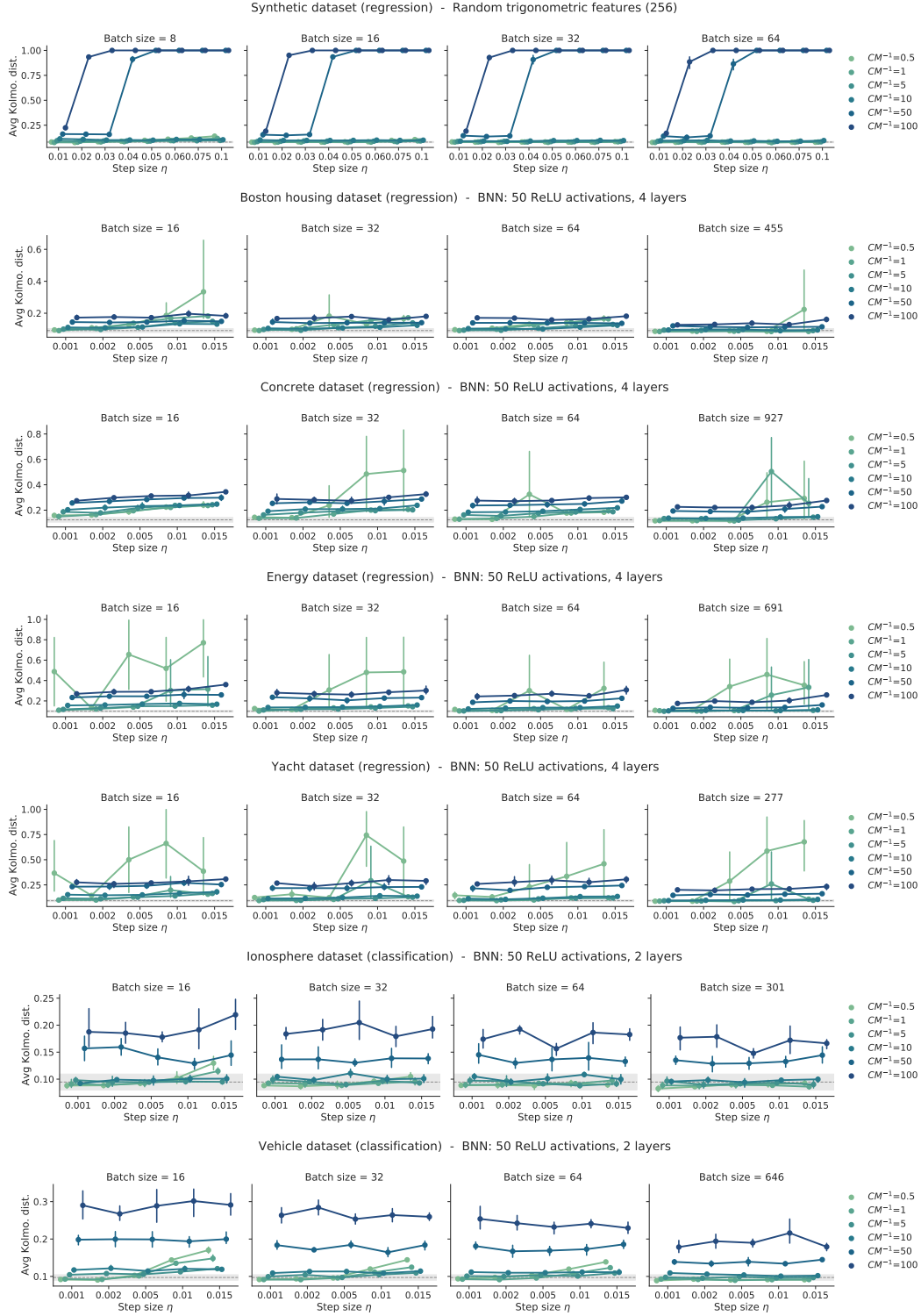


Figure 11: Exploration of step size and batch size for different values of the product CM^{-1} , where we set $M = \tilde{V}$. The grey dotted line denotes the self-distance for the distribution of the oracle. The LEAPFROG integrator is used in all cases.